2014

Design of a Passive Exoskeleton Spine

Haohan Zhang
University of Massachusetts Amherst

DESIGN OF A PASSIVE EXOSKELETON SPINE

A Thesis Presented

by

HAOHAN ZHANG

Submitted to the Graduate School of the
University of Massachusetts Amherst in partial fulfillment
of the requirements for the degree of

MASTER OF SCIENCE IN MECHANICAL ENGINEERING

September 2014

Department of Mechanical and Industrial Engineering

DESIGN OF A PASSIVE EXOSKELETON SPINE

A Master's Thesis Presented

by

HAOHAN ZHANG

Approved as to style and content by:

_____
Frank C. Sup IV, Chair

_____
Kourosh Danai, Member

_____
Brian R. Umberger, Member

_____
Donald Fisher, Department Head as Department
of Mechanical and Industrial Engineering

DEDICATION

To family

ACKNOWLEDGMENTS

I would like to express my deepest appreciation to my advisor, Professor Frank Sup, for all his guidance and assists on my research. He introduced me to access the path of how to do research professionally, which was not only significant for my thesis accomplishment but also will be a great wealth for my future research work. Also, I would like to appreciate my committee faculties, Professor Kourosh Danai and Professor Brian Umberger, for their efforts and advice to lead me to a successful thesis work.

I would like to thank everyone I was working with in the Mechatronics and Robotics Research Laboratory (MRRL), for their helpful and kind assists on my research work. I want to thank Andrew Kennedy Lapre and Abhijit Kadrolkar for their assists in terms of the instructions on simulation and biomechanics data collections. I also want to thank Matthew Charles Ryder and Jonathan Cummings for their guidance on prototype fabrications.

ABSTRACT

DESIGN OF A PASSIVE EXOSKELETON SPINE

SEPTEMBER 2014

HAOHAN ZHANG, B.E.M.E, DALIAN UNIVERSITY OF TECHNOLOGY

M.S.M.E., UNIVERSITY OF MASSACHUSETTS AMHERST

Directed by: Professor Frank C. Sup IV

In this thesis, a passive exoskeleton spine was designed and evaluated by a series of biomechanics simulations. The design objectives were to reduce the human operator's back muscle efforts and the intervertebral reaction torques during a full range sagittal plane spine flexion/extension. The biomechanics simulations were performed using the OpenSim modeling environment. To manipulate the simulations, a full body musculoskeletal model was created based on the OpenSim *gait2354* and "lumbar spine" models. To support flexion and extension of the torso a "push-pull" strategy was proposed by applying external pushing and pulling forces on different locations on the torso. The external forces were optimized via simulations and then a physical exoskeleton prototype was built to evaluate the "push-pull" strategy *in vivo*. The prototype was tested on three different subjects where the sEMG and inertial data were collected to estimate the muscle force reduction and intervertebral torque reduction. The prototype assisted the users in sagittal plane flexion/extension and reduced the average muscle force and intervertebral reaction torque by an average of 371 N and 29 Nm, respectively.

TABLE OF CONTENTS

Page

ACKNOWLEDGMENTS v
ABSTRACT vi
LIST OF TABLES viii
LIST OF FIGURES ix

CHAPTER

1. THESIS INTRODUCTION 1
    1.1 Research Motivation 1
    1.2 Scope 1
    1.3 Thesis Outline 2
2. THESIS BACKGROUND 4
    2.1 The Human Spine 4
    2.2 Biomechanical Modeling and Simulation 6
    2.3 Prior Researches on Exoskeleton and Musculoskeletal Humanoids 7
3. SAGITTAL PLANE SPINE FLEXION/EXTENSION RECONSTRUCTION OF A HUMAN SUBJECT VIA BIOMECHANICS SIMULATIONS 11
    3.1 Motion Capture and Data Collection 11
    3.2 Model Establishment 12
    3.3 Dynamic Movement Reconstruction 14
    3.4 Result Validation 16
4. A "PUSH-PULL" EXTERNAL ASSIST STRATEGY FOR THE HUMAN TORSO 21
    4.1 The "Push-Pull" External Assist Strategy 21
    4.2 Validation via Biomechanics Simulation 23
5. OPTIMIZATION OF THE ELASTIC ELEMENTS IN THE "PUSH-PULL" ASSISTIVE STRATEGY 28
    5.1 Optimizing the "Push-Pull" Strategy 28
    5.2 Optimization by Monte Carlo via Matlab Scripting and OpenSim Simulation 29
        5.2.1 Simulation Set Up 29
        5.2.2 Optimization Results 30
    5.3 Result Estimation and Analysis 32
6. REALIZING THE "PUSH-PULL" ASSISTIVE STRATEGY 38
    6.1 Physical Modeling 38
    6.2 Prototype Fabrication 40
7. PROTOTYPE EVALUATION 42
    7.1 Experiment Setup 42
    7.2 Dynamic Evaluation 45
    7.3 Results Comparison for Dynamic Tests 47
    7.4 Results Comparison for Static Tests 53
8. CONCLUSION 61
APPENDIX: FULL DYNAMIC TESTING RESULTS FOR SUBJECTS NO. 2 AND 3 64
BIBLIOGRAPHY 66

LIST OF TABLES

Table Page

3.1: Involved muscle modeling details 14

5.1: Correlation coefficients between the spring forces and the Back Muscle Effort and the Intervertebral Reaction Torque reductions 35

6.1: Optimized spring constant in biomechanics simulation 40

6.2: Specification of the extension springs applied in the prototype 41

7.1: Subject physical properties 43

7.2: Experiment Tasks List 44

7.3: Sensor number remained during tests wearing exoskeleton for different subjects 44

7.4: Stable torso bending angle $\boldsymbol{\theta}$ at different positions for each subject (Units: degree). The reference height in **Figure** 7.2 for each subject in different trials are listed in **Table** 7.2.....57

7.5: Average percentage of sEMG reduction of each channel for each subject. The largest reductions among all three subjects at lumbar and thorax level muscles are marked bold. 58

7.6: Spring length measurements during the static test of Subject No. 1 (Units: m) 59

7.7: Spring length measurements during the static test of Subject No.2 (Units: m) 59

7.8: Spring length measurements during the static test of Subject No.3 (Units: m) 59

7.9: Result estimation for each subject 60

LIST OF FIGURES

Figure Page

2.1: Current exoskeleton and relative robotics research achievements (a) BLEEX for load transporting; (b) HAL-5 designed for health care workers; (c) Passive second spine concept proposed for transferring load from shoulder to pelvis; (d) Kenshiro full body artificial musculoskeletal humanoid robot; and (e) MIT Cheetah implemented a flexible spine for high speed running 8

3.1: Location of motion capture markers 12

3.2: Full body skeletal model establishment flow and customized model in OpenSim. 13

3.3: Computed kinematics of hip flexion and gross spine flexion/extension in simulation. 15

3.4: Computed kinematics of each level of intervertebral joint in simulation. 15

3.5: Computed total back muscle actuation forces during flexion/extension in simulation. 16

3.6: Computed intervertebral torques during flexion/extension in simulation. 17

3.7: Computed joint reaction force during flexion/extension in simulation (a) compression; and (b) shearing 19

3.8: Configuration of full spine flexion/extension in the OpenSim 20

4.1: Mathematical model of "push-pull" external assist strategy 22

4.2: "Push-pull" implementation using biomechanics model in OpenSim 23

4.3: The total back muscle force with different TS constant and zero LS constant 25

4.4: The intervertebral torques at L5-S1 level with distinct Thorax Spring constants and zero Lumbar Spring constant 26

4.5: The intervertebral reaction torques in lumbar at L_5-S_1 with identical Thorax Spring constant (6000 N/m) and distinct Lumbar Spring constants 26

4.6: The total muscle activation forces with identical Thorax Spring constant (6000 N/m) and different Lumbar Spring constants 27

4.7: The compression (Fy) and shearing (Fx) reaction forces without Thorax Spring and Lumbar Spring comparing with the ones with Thorax Spring and Lumbar Spring 27

5.1: Flowchart of optimization via Matlab scripting OpenSim simulations 30

5.2: The relationship between the Back Muscle Effort and the spring constants 31

5.3: The relationship between the Intervertebral Reaction Torque and the spring constants 31

5.4: The weight plot for seeking the optimal spring constants 32

5.5: The comparison of the computed total muscle activation force between with the optimal spring constants and the natural body 33

5.6: The comparison of the computed intervertebral torque at L_5-S_1 lumbar level between with the optimal spring constants and the natural body 33

5.7: The maximum reaction forces (compression at L_5-S_1, shearing at L_1-L_2) in lumbar with the optimal spring forces 34

5.8: The optimal spring forces: (a) the pulling force, and (b) the pushing force 35

5.9: Relationships between each objective reduction and individual spring force 36

6.1: 3D physical model for passive exoskeleton spine suit: (a) view of wearing on user; (b) view zoomed in of wearing on user; (c) back view of the suit; (d) mechanism details. 39

6.2: The cable-tendon mechanism of applying the pushing spring force on the human back: (a) mechanism sketch; (b) side view of 3D model. 41

7.1: (a) EMG sensor distributions on the back of subject; (b) and (c) configurations of the subject wearing the exoskeleton spine prototype. 43

7.2: Static test setup 45

7.3: Dynamic model for subject flexion with EMG and inertial sensor attached 46

7.4: sEMG signal processing. (a) Detrended; (b) high pass filtered at 2 Hz; (c) low pass filtered at 450 Hz; (d) normalized; (e) rectified; and (f) low pass filtered at 3 Hz to find envelope.48

7.5: Low-pass filtered sEMG comparing with no low-pass filtered signal.....48

7.6: (a) Angle comparison from sensor 8 at T_{11} level in both with/without exoskeleton; and (b) linear accelerations on x and z direction with exoskeleton from sensor 7 at T_{11} level ...50

7.7: The linear accelerations on x and z directions from channel 7 at T_{11} level with/without exoskeleton 50

7.8: sEMG comparison of Subject No. 1 in the dynamic tests with/without exoskeleton – 60-second long continuous sEMG comparison. 51

7.9: sEMG comparison of Subjects in the dynamic tests with/without exoskeleton: (a) Subject No. 1; (b) Subject No. 2; (c) Subject No. 3. 52

7.10: Comparison of angle in different static test trials from channel 7: (a) Subject No. 1; (b) Subject No. 2; (c) Subject No. 3. 54

7.11: Comparison of linear accelerations in different static test trials from channel 7: (a) Subject No. 1; (b) Subject No. 2; (c) Subject No. 3.....55

7.12: Comparison of sEMG in different static test trials of Subject No. 1 56

7.13: Comparison of sEMG in different static test trials of Subject No. 2 56

7.14: Comparison of sEMG in different static test trials of Subject No. 3 57

A.1: Results comparisons of dynamic tests for Subject No.2: (a) angle comparison at T_{11} level; (b) linear accelerations at T_{11} level wearing exoskeleton; (c) sEMG comparison at channel 2, 4, 7 and 8.....64

A.2: Results comparisons of dynamic tests for Subject No.3: (a) angle comparison at T_{11} level; (b) linear accelerations at T_{11} level wearing exoskeleton; (c) sEMG comparison at channel 2, 4, 7 and 8.....65

CHAPTER 1

THESIS INTRODUCTION

1.1 Research Motivation

A strong, yet flexible, torso allows the humans to achieve upright walking, bear external loads and perform many other versatile movements. However, due to aging, injuries and long-term physical laboring, the health of the spine and supporting muscles can be compromised and dramatically reduce the quality of life for individuals To restore mobility, exoskeletons are becoming a reality for assisting people with spinal cord injury and rehabilitation, but few of them focus on supporting the torso. Therefore, this thesis focus is on the design of a passive spine exoskeleton to assist in sagittal plane movements. In addition, this thesis uses biomechanics simulations to guide the mechanical design to better account for the complexity of the human spine and its supporting musculature.

1.2 Scope

The research object of this thesis is to develop a biomechanics simulation capable of guiding the design of an exoskeleton to support the human spine during sagittal plane movements. The design targets are to reduce the muscle forces and intervertebral reaction torques. The research focuses on the sagittal plane spine flexion/extension that the subject moves symmetrically. Therefore, only the major muscle group responsible for sagittal plane movement – the erector spinae – is included in the scope. In addition, the spine in this thesis refers to thoracolumbar and not the cervical spine. Comparing the Range Of Motion (ROM) of the lumbar, the thorax is considered to be a lumped mass. Since the hip joints contribute to motion of the torso, their motions are also studied and used to drive the passive exoskeleton.

Several models were used for different goals throughout the entire thesis. The fundamental musculoskeletal model was developed in OpenSim, which is a validated simulation platform for biomechanics studies. In addition, mathematical modeling was used to simplify the biomechanics model and propose potential external assists. This external assistive strategy was evaluated and optimized in OpenSim by applying spring forces onto the musculoskeletal model. A dynamic model was applied to estimate the muscle forces and intervertebral torques *in vivo*, which was based on the sensor coordinate system.

The work was performed in the Mechatronics and Robotics Research Laboratory (MRRL) at the University of Massachusetts Amherst and advised by Professor Frank Sup. The biomechanics study was collected at the Biomechanics Laboratory at the University of Massachusetts Amherst. The simulation work was performed in OpenSim modeling environment, and programmed in MATLAB. The physical model was designed in the Autodesk Inventor modeling environment.

1.3 Thesis Outline

This this is organized as follows. **Chapter** 2 presents the background material, including biomechanics of human spine system, current exoskeleton designs, compliant structures used in robotics, and biomechanics simulation.

Chapters 3 and 4 present the biomechanics data collection and simulations used in this thesis. **Chapter** 3 describes the kinematics collection using high speed motion capture cameras and reconstruction in biomechanics simulations using a full-body musculoskeletal model. The model is compared with spine biomechanics studies in the literature. The muscle forces and joint reactions are computed and used as the basis for this research. A mathematical model is developed in **Chapter** 4 using the developed musculoskeletal model. It considers the human body as a multi-

link inverted pendulum in sagittal plane, of which the lumbar is an integral yet pliable link. A "push-pull" assistive strategy is then proposed according to this mathematical model which generates a pulling force between the thorax and pelvis via the elongation of backside of the lumbar and applies a pushing force on the lumbar to compensate the lumbar reaction torques. The "push-pull" is realized by two spring forces in the musculoskeletal model and evaluated through biomechanics simulations with different spring constant combinations.

Chapters 5 through 7 cover the mechanical design phase. In **Chapter** 5, the design parameters of the elastic elements are optimized using MATLAB scripting and OpenSim simulations, to minimize the muscular effort and intervertebral reaction torques. A Monte Carlo approach is applied to this multi-objective optimization problem. **Chapter** 6 realizes the physical implementation of the "push-pull" strategy in mechanical design and a physical prototype is constructed. In **Chapter** 7, the results of *in vivo* prototype testing are shown. Surface electromyography (sEMG) and inertial signals were recorded with and without the spine exoskeleton prototype on three different subjects. The thesis is concluded with **Chapter** 8 with discussion of contributions of the thesis and future work.

CHAPTER 2

THESIS BACKGROUND

2.1 The Human Spine

The human spine connects the skull and pelvis and consists of a series of vertebrae, tissues, ligaments and muscles. The vertebrae link to create the vertebral column that provides rigidity of torso and protects the spinal cord and nerve roots in addition to carrying loads [1]. Additionally, the spine is flexible and can support bending moments with intervertebral discs which are pliable tissue and connect each vertebra to each. The properties of the intervertebral joints are defined by compliance of the discs [1]–[3]. Although the vertebrae are separated by discs, they articulate through a locking mechanism called a Zygapophyseal joint, which is located posteriorly of each vertebrae. These posterior elements constrain the movement of each vertebrae to protect the intervertebral discs [1]. These joints and ligaments endow the vertebral column with passive properties and certain stabilities and its active movement is controlled by different groups of muscles.

The spine column comprises four major sections (from the top to the bottom): cervical, thorax, lumbar and sacral. The cervical spine controls skull motion, supports the load from head, and generates reaction forces of the neck muscles; the thorax mainly protects and supports the inside organs; the lumbar spine contributes to most of the torso movement, and lastly the fused sacral connects the spine with the pelvis and does not contribute to the spine motion. The cervical spine was excluded in the research scope since the concern of this thesis was on the back mobility and loading capability. The thoracolumbar naturally forms an *"S"* shape since the child first learn

upright walking. This curvature helps distribute body mass away from the straight line between skull and pelvis, absorbs the shocks and minimizes the muscle activity during locomotion [1], [4].

Overall, the spine undertakes three major motions: sagittal plane flexion/extension, lateral bending and axial rotation, of which the sagittal plane flexion/extension is the most significant in terms of ROM. In this case, the sagittal plane flexion/extension is the major consideration in this thesis. On the other hand, the substantial sagittal plane flexion/extension is coupled with movements of the hip, thus the hip flexion is also included in this study.

The movement of the spine is primarily actuated by three groups of muscles which surround the lumbar spine to stabilize and control the most ROM of thoracolumbar. Throughout a large amount of past anatomical studies [1], [5]–[7], the muscles are located in three different groups: (1) the intersegmental muscles, (2) the anterolateral muscles consisting of psoas major (PM) and quadratus lumborum (QL), and (3) the posterior muscles comprised of multifidus, longissimus thoracis pars lumborum (LTpL), iliocostalis lumborum pars lumborum (ILpL), longissimus thoracis pars thoracis (LTpT) and iliocostalis lumborum pars thoracis (ILpT). Of the muscle groups, the posterior muscles are principal with respect to controlling the spine movement.

The spine's structure and actuation enable human upright walking and other daily tasks, nevertheless the system is vulnerable to degradation over one's lifetime and external loading. Age gradually and inevitably weakens the biological tissues in the system. The skeletal as well as muscle-tendon cells become less efficient and slower with respect to renew and repair. As a consequence, the spine movement is substantially restricted and the capability decreases [1], [3], [8], [9]. Despite aging, intense labor working also damages the spine system. For instance, excessive loading on spine during lifting generates larger joint reaction torque in intervertebral discs to compensate the insufficient force provided by the muscles [1], [8], [10], [11]. With this

motivation, this thesis seeks to investigate how external assistance can compensate the insufficiency of muscles and minimize the intervertebral joint reaction torques.

2.2 Biomechanical Modeling and Simulation

The human spine in conventional humanoid gait studies has been modeled as a single rigid link. This is because of incomplete system identification and the relatively high computational cost to capture the complexity of the spine. As a result, there is no movement within spine region and therefore all torso motions are associated with hip movement. Unlike the human limbs, the structure inside torso is complex. Alternatively, the system including vertebrae, discs, tendons and muscles are hidden and dynamically coupled under the skin. In this case, modeling of the spine system according to *in vivo* experiments is very difficult. As such, most dynamic models are established through combining anatomy with movement science, which applies biomechanics methods such as motion capture to gain movement details and surface electromyography (sEMG) techniques to estimate muscle forces and intervertebral reaction torque *in vivo*.

Most biomechanical lumbar spine models using multiple groups of muscles are indeterminate because there are more unknown forces than independent equations. There are three major approaches built up to settle the indeterminate problem: mathematical optimization [2], [12], sEMG assisted, and sEMG assisted by optimization [2], [5], [12]. The sEMG assisted by optimization approach balances intervertebral reaction torques as well as the individual muscle activation strategies [12].

Biomechanics simulations are an effective component of movement science which mainly depends on observations [13], [14]. OpenSim is an open source biomechanics simulation platform that provides the capability to reconstruct motion. It assists researchers' review and analysis of the activities of the musculoskeletal system. OpenSim includes biomechanics algorithms such as

inverse kinematics, computed muscle control and forward dynamics for a user to simulate and compute the kinematics, muscle activations and reaction forces for the customizable musculoskeletal models. Therefore, the musculoskeletal activities of the specific model corresponding to specific subject can be observed within simulations in different external environment based on given movement tasks. It is an extremely promising tool for the development of human-machine interfaces to generate and optimize designs prior to human subject testing. The open source platform encourages sharing between researchers and the team at UC Berkeley has recently developed and validated a fully detailed musculoskeletal lumbar spine model [6], [7]. In summary, biomechanics simulation is a necessary tool for guiding the design process and has been applied in this thesis.

2.3 Prior Researches on Exoskeleton and Musculoskeletal Humanoids

Exoskeletons for rehabilitation and military usage have become increasingly a reality. By applying torques and forces from actuators in parallel with the human joints, an exoskeleton can extend or restore the motion and/or load capacity of operator. An early example is the Berkeley Lower Extremity Exoskeleton (BLEEX) intended for military load carrying [15], [16]. The most advanced research exoskeleton is the Hybrid Assistive Limb (HAL) that is designed both for healthy individuals and impaired individuals to augment their abilities with a wearable suit [8], [17]–[20]. A passive spine exoskeleton concept called Second Spine developed at Columbia University aims to enhance load carrying on back [21].

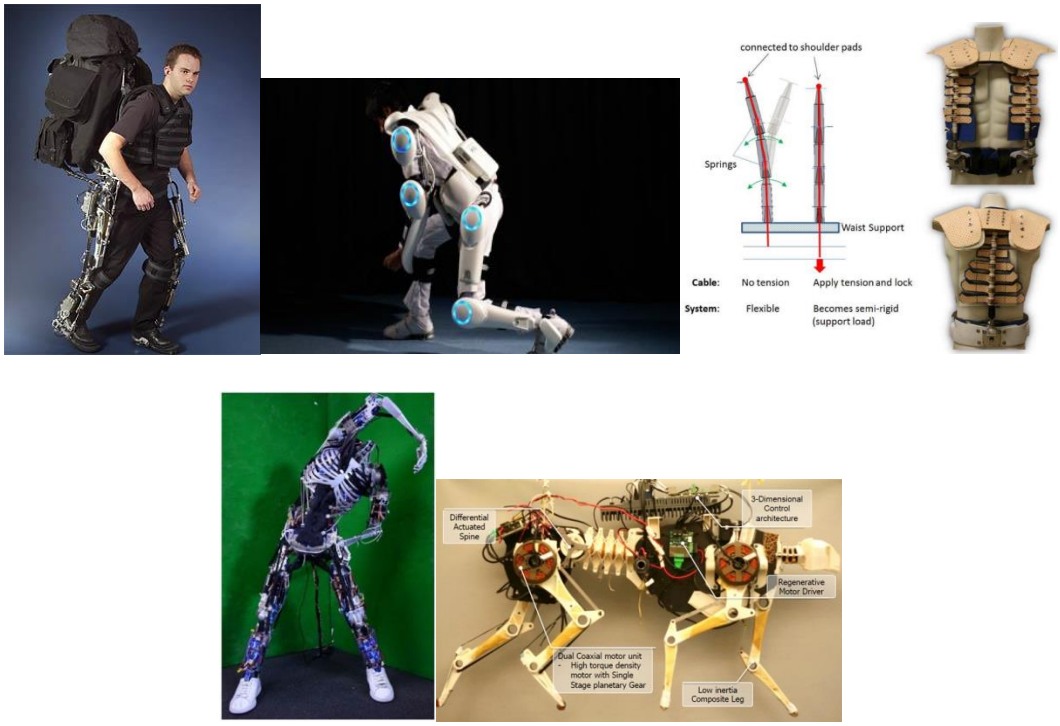

Figure 0.1: Current exoskeleton and relative robotics research achievements (a) BLEEX for load transporting; (b) HAL-5 designed for health care workers; (c) Passive second spine concept proposed for transferring load from shoulder to pelvis; (d) Kenshiro full body artificial musculoskeletal humanoid robot; and (e) MIT Cheetah implemented a flexible spine for high speed running

BLEEX shown in **Figure** 2.1 (a), is designed to provide a solution for legged locomotion on heavy object transportation such as staircases and rocky terrains by transferring the payload to ground. It can be worn on the operator and extend the load capability of the operator with a rigid load hook mounted on user pelvis [16]. It consists of two anthropomorphic legs actuated by double-acting linear hydraulic actuators and a rigid back frame for mounting the payload. In total, it maintains 7 DOFs on each leg, while only 4 of which are actuated (flexion/extension at the ankle, knee, and hip and abduction/adduction at the hip). The control algorithm increases the closed loop system sensitivity to its wearer's forces and torques without any measurement from the wearer, while maintaining the advantages of wide bandwidth maneuvers and unaffected by changing human dynamics with a tradeoff that a highly accurate model is necessary.

The HAL exoskeleton suit, shown in **Figure** 2.1 (b), consists of a lower body and upper body component that can be combined to create a full-body suit. It is being developed by Professor Sankai at the University of Tsukuba, Japan. Compared with prior work, the latest version, dubbed HAL-5 [20], was designed to strengthen the shoulder for the health care workers. The bioelectrical signal [17], [18] was used to recognize the user intent and control the device. To offer help for lower back pain, a passive mechanism was introduced with a rigid corset associating with the motion of the hip [8], while the rigid corset constrained the ROM of the user. Recently, they proposed a spine exoskeleton (exo-spine) concept [19] that applies tendon driven actuation to couple the multiple exoskeleton vertebrae motion. This exo-spine can increase the wearer's loading capability, however, it does not provide details in terms of the muscle efforts and joint reactions of the user's spine.

The Second Spine, in **Figure** 2.1 (c), is a concept by Robotics and Rehabilitation Laboratory at Columbia University. It was designed to achieve wearable load carrying by transferring loads from shoulders to pelvis. By means of a simple manual adjustment, this passive device can switch the loadbearing mode from high stiffness to high flexibility/compliance [21].

Meanwhile, several relative contributions have been achieved in the robotics field, for instance, the full body biological inspired robot such as Kenshiro [22]–[24], and the elastic spine to pursue high robot speed running performance such as the MIT Cheetah [25], [26]. Humanoid Kenshiro illustrated in **Figure** 2.1 (d) is a novel of humanoid robot which copies the muscular skeleton from the human being [24]. It uses 5 series articular vertebrae lumbar with 2 DOFs (flexion/extension and lateral bending) associating a solid construction of thorax. Moreover, it is tendon driven by actuators where the tendons perform the elastic artificial muscles. The latest version of MIT Cheetah shown in **Figure** 2.1 (e) uses flexible spine to connect front and rear body

and conserve energy during high speed robot running [26]. It maintains a high flexibility with the passive arch shape spine during running.

In summary, exoskeleton suits provide a viable solution to externally assist human movement, either passively or actively. More recent devices have started to emphasize the function of a compliant spine in movements and implementing flexible structures in their designs. However, there are no principles that effectively guide such a design process. In addition, although current exoskeletons can augment user loading capabilities, data is lacking on how muscle forces and intervertebral reaction torques are affected. Therefore, this thesis aims to fill these knowledge gaps.

CHAPTER 3

Sagittal Plane Spine Flexion/Extension Reconstruction of a Human Subject via Biomechanics Simulations

Abstract – In this chapter, a series of biomechanics simulations were conducted to reconstruct a specific movement – spine flexion/extension in sagittal plane of a subject. The motion capture was used to collect the kinematics information of the subject. These motions were used to drive a customized musculoskeletal model in OpenSim. Additionally, the muscle actuation forces and joint reactions were computed via forward simulations. The forward simulation results were then evaluated by comparing with prior published literature and were used to assist the design of a passive exoskeleton as described in **Chapters** 5-7.

3.1 Motion Capture and Data Collection

This study involved human participants and was approved by the University of Massachusetts – Institutional Review Board (IRB). The test subject for this study was a 25-year-old, healthy male, 165 cm tall and 63kg. The motion capture and relative surface Electromyography (sEMG) data collection took place in the Biomechanics Laboratory at the University of Massachusetts Amherst.

An eleven-camera Qualisys Oqus 3-Series optical motion capture system was used to capture the experimental marker kinematics. Motion capture markers were placed on the subject, as shown in **Figure** 3.1. The subject was required to start with a natural stance, flex forward approximate 90 degrees, and extend back to stance position. During the experiment, the subject was asked to finish several trials in a minute continuously with a consistent speed according to a timer beeping. The motion speed was set to be 3-second-flexion and 3-second-extension. All later

simulations and designs were based on the best captured trial (all marker coordinates were captured).

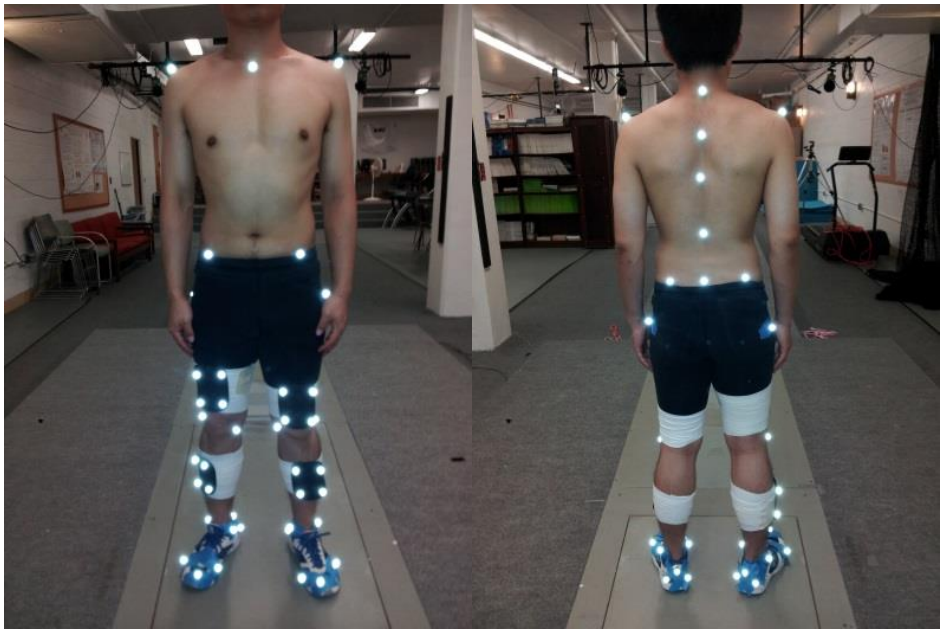

Figure 0.1: Location of motion capture markers

3.2 Model Establishment

It is known that the ankle and hip joints are involved in a full range spine flexion/extension movement and help maintain balance. Already developed in OpenSim are base models, such as the *gait2354* model which is a detailed lower limb musculoskeletal model with a rigid torso skeleton for gait study. Also, a musculoskeletal lumbar spine model [6], [7] has been developed at UC Berkeley, which has a 3-DOF flexible lumbar spine pin jointing a 1-DOF of axial rotational thorax spine. However, individually applying each of them cannot satisfy the requirements in this spine study during the full body movement.

Therefore, a combined upper and lower body model was created. A sketch indicating the model construction is shown in **Figure** 3.2, where the arrows represent the hierarchy flow of the bones and always point from the child body to the parent. Since there was no movement of both

feet in this study, they were fixed to the ground instead of applying with ground reaction forces. This minimized the computational efforts and data noise. In this case, the root joint which was used to connect the model body to ground was defined as a weld joint between the right foot with the ground (shown as the black solid triangle in **Figure** 3.2), then the higher level bones were jointed with the corresponding lower level parent via ankle, knee, and hip on the right side till pelvis. Thereafter, the lower level bones on the left side were oppositely jointed with their upper parents to finish the lower body skeleton. Additionally, the modified flexible lumbar spine [6], [7] whose pelvis and hip joints had been removed was welded to the top of the pelvis with the sacrum. Since movement occurred only in the sagittal plane, the other planes of movements (frontal and coronal) were locked to simplify the model.

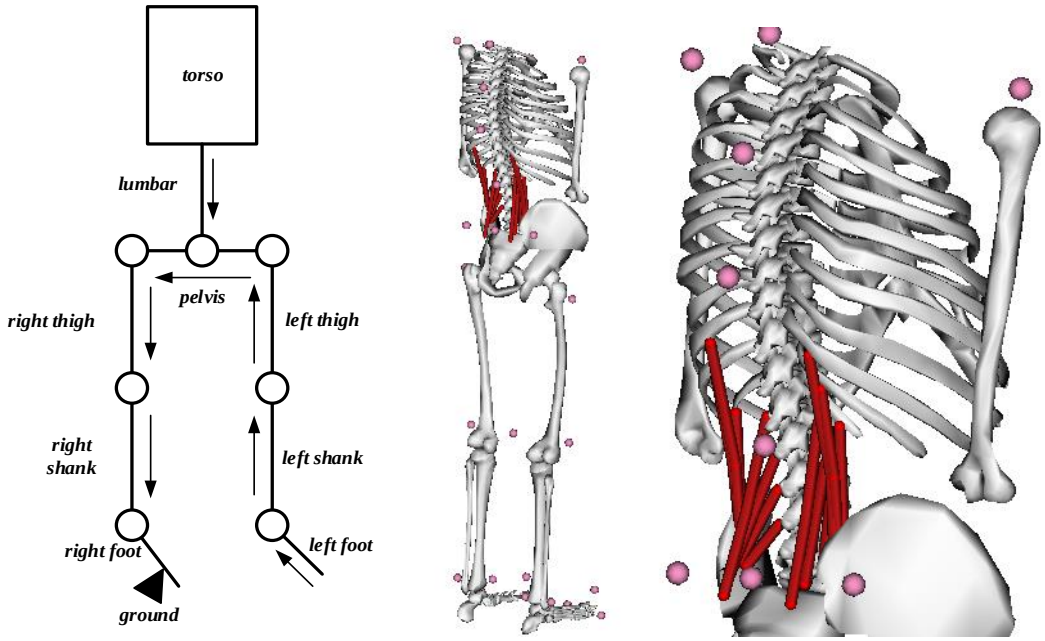

Figure 0.2: Full body skeletal model establishment flow and customized model in OpenSim.

After redefining the bodies and joints of the skeleton model, the back muscles were added to the model. Seven erector spinae on each side were inherited from the musculoskeletal lumbar model, as listed in **Table** 3.1. These muscles are major muscles with respect to undertaking sagittal

plane spine flexion/extension according to [1], [6], [7]. Instead adding lower limb muscles, the ideal torque actuators were applied to actuate those joints in simulations. Reducing the number of muscles, simplifies the modal and thus the computational cost without affecting the validity of the model. The combined musculoskeletal model is shown in **Figure** 3.2. Last, the model was scaled to the subject size for accuracy, according to the static measurements on the subject.

Table 0.1: Involved muscle modeling details

Muscle Name	Max Isometric Force (N)	Optimal Fiber Length (m)	Tendon Slack Length (m)	Pennation Angle at Optimal (rad)
$ILpL^b - L_1$	50	0.0515	0.109	0.241
$ILpL^b - L_2$	71	0.0373	0.0789	0.241
$ILpL^b - L_3$	84	0.0252	0.0533	0.241
$ILpL^b - L_4$	87	0.0167	0.0354	0.241
$ILpT^a - T_{10}$	46	0.131	0.0692	0.241
$ILpT^a - T_{11}$	57	0.116	0.0506	0.241
$ILpT^a - T_{12}$	68	0.0890	0.0366	0.241

3.3 Dynamic Movement Reconstruction

OpenSim provides the **Inverse Kinematics Tool** to calculate the coordinate kinematics of the model by aligning the experimental markers to the model markers. The model markers were visually added into the model according to reference photos mentioned previously. After running the algorithm multiple times and endowing joints with proper weights, the least marker errors were achieved for the entire range of motion. Of all the coordinates, the gross spine flexion/extension (shown in **Figure** 3.3) was the most important, because it revealed the action of the spine during flexion. Here the gross spine flexion/extension referred to the deflection of the thoracic spine segment T_{12} relative to the sacrum S_1 according to [6], [7] during spine flexion/extension. Hip flexion (shown in **Figure** 3.3) was also important as it connected the upper body with the lower limbs which were involved during the movement. Both magnitudes of the hip flexion and the gross

spine flexion/extension increased from natural stance and reached their peak at the full range flexion, and then decreased when the model returned to vertical stance. In addition, the linear relationship between the overall flexion/extension and the rotation of each lumbar vertebrae flexion angle can be calculated according to [6], [7], [11] and is plotted in **Figure** 3.4.

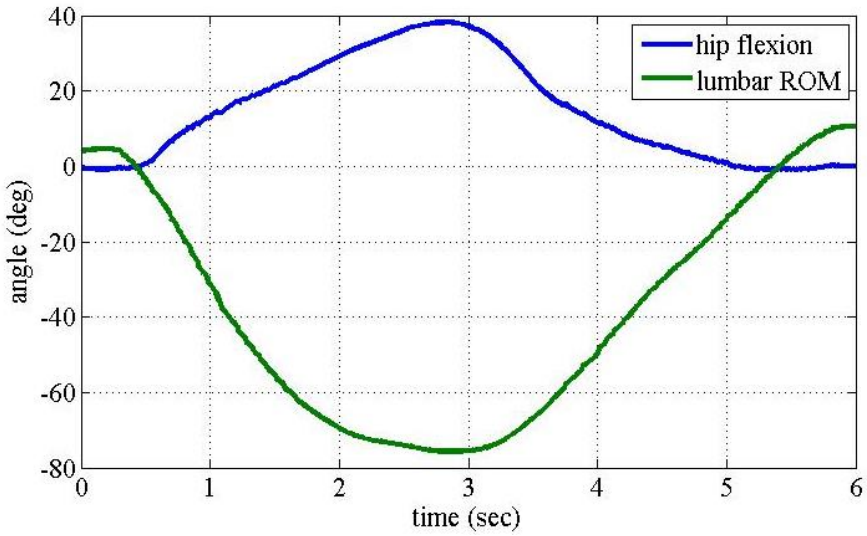

Figure 0.3: Computed kinematics of hip flexion and gross spine flexion/extension in simulation.

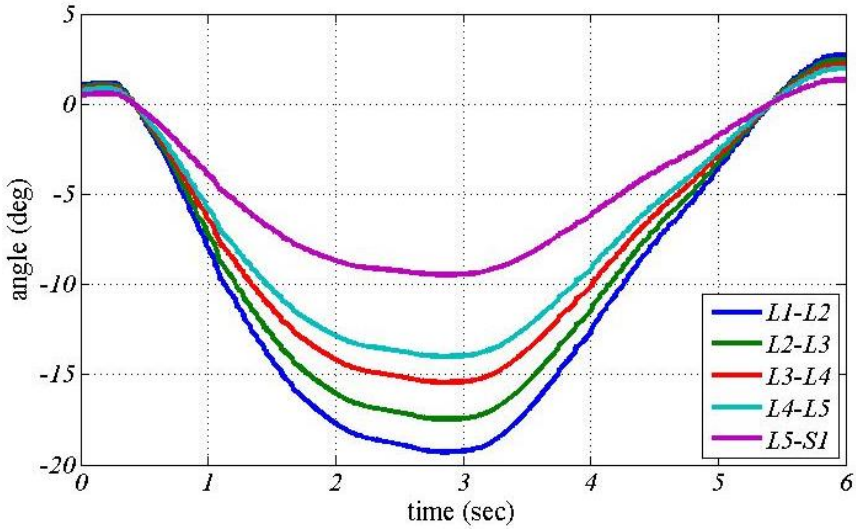

Figure 0.4: Computed kinematics of each level of intervertebral joint in simulation.

The **Residue Reduction Algorithm (RRA)** was applied to minimize the large residue forces caused by effects of modeling and marker errors [13], [14], where the torso was set as the

adjusted body. After running this algorithm, this new model obtained a better mass distribution. The **Computed Muscle Control (CMC)** is an approach to compute the muscle actuation force via tracking the inputted kinematics [13], [14]. CMC was applied to this full body model with the simplified muscle profile to compute the actuation force versus time for each muscle at each time point. This enabled the muscle actuation details to be simulated and examined. Furthermore, the **Joint Reaction Analyses**, a plugin in OpenSim that allows the user to compute the joint load [13], [14], was designed to compute the intervertebral reaction torques. Both the computed muscle forces and the intervertebral reaction torques were applied as the design objectives to be minimized.

3.4 Results

The total actuation force to articulate the spine is illustrated in **Figure** 3.5 and shows the sum of all the muscle forces. The intervertebral reaction torques at all sublevels of lumbar are shown in **Figure** 3.6 during the full range flexion/extension. Both the muscle force and intervertebral torque increase during the forward flexion and reach a peak at the full range flexion.

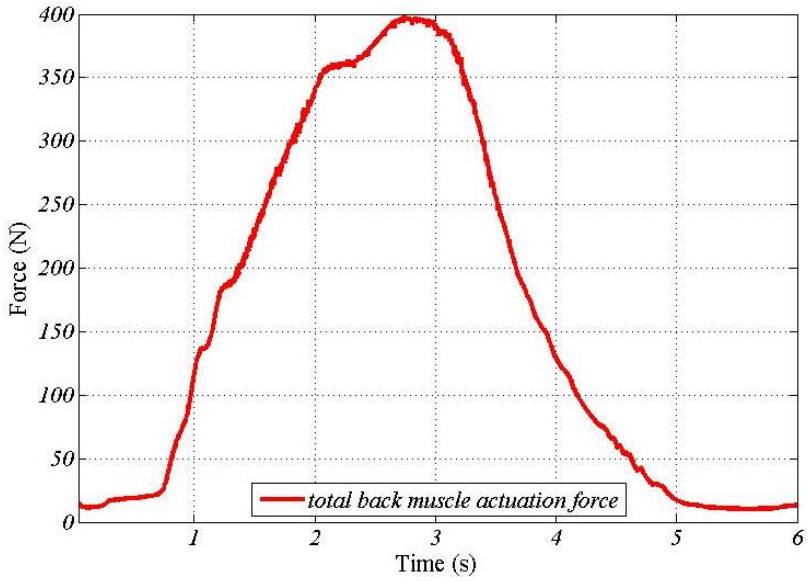

Figure 0.5: Computed total back muscle actuation forces during flexion/extension in simulation.

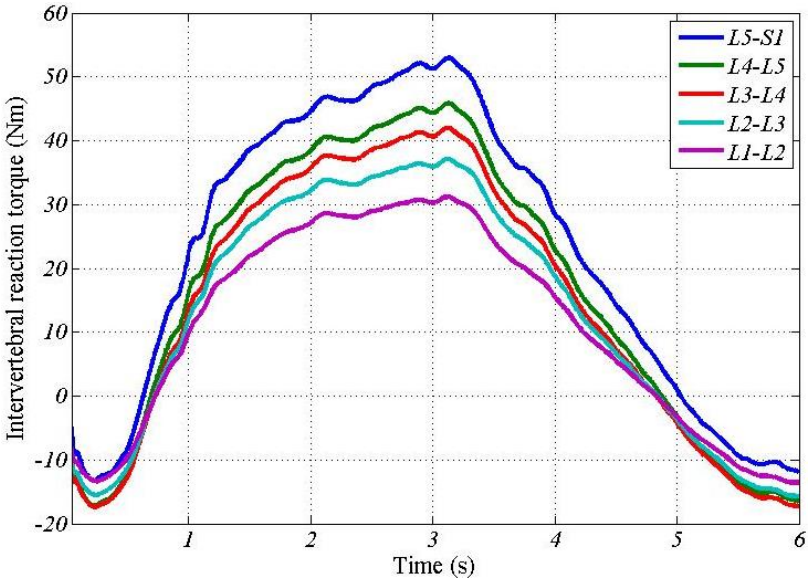

Figure 0.6: Computed intervertebral torques during flexion/extension in simulation.

Referring to [1], the dorsal muscles are activated during spine flexion to provide extensive torque on the torso to hold it upright. In addition, it should be noticed that during the flexion period (from 0 – 3 seconds, approximately) the computed muscle forces increase slower with the flexion angle, which can be explained by erector spinae muscle flexion-relaxation. According to[1], [27], the myoelectric activity in the erector spinae muscles increases at the beginning of flexion and then decreases when close to fully flexed. At this point, the forces need to maintain the equilibrium at the full range flexion are provided by passive muscle tissue, tendons and ligaments. Since OpenSim uses the "Hill" muscle model which includes passive mechanisms, the simulation result of the total back muscle force illustrated in **Figure** 3.5 align with theory. The computed muscle activation force, however, is much smaller than reality due to the simplified muscle profile.

Meanwhile, the contractions of the muscles generate reaction forces on the posteriors sides of the intervertebral discs, and therefore produce a posterior intervertebral reaction torque at each level of lumbar disc, illustrated in **Figure** 3.6. According to some studies [1], [28], these reaction torques are the major source causing the lower back pains.

In addition to the intervertebral reaction torques, there also exists the compression and shearing during the spine flexion/extension. **Figure** 3.7 shows the computed compression and shearing in local reference frame and the magnitudes of resultant reaction forces according to the compression and shearing in the simulation. The compression within lumbar discs increases with the flexion angle due to larger muscle contraction forces. In the human spine, the vertebrae and discs are designed to resist large compression (range 2 – 14 KN), while the shearing are mostly loaded by the posterior Zygapophyseal joints or compensated by the intra-abdominal pressure by average 2 KN (range 0.6 – 2.8 KN) before performing on the intervertebral discs which can also bear shearing between 380 and 760 N [1]. However, there was no such definitions in the OpenSim and so was the full body musculoskeletal model. Therefore, when estimating shearing, the intrinsic dynamics of this musculoskeletal model should be emphasized. Since the muscles majorly parallels the spine curve, the angles formed by each two adjacent vertebrae determine the shearing during flexion against gravity. According to the kinematic at each level of lumbar in **Figure** 3.4 and configuration of model flexion in **Figure** 3.8, the higher level lumbar vertebrae are more "parallel" to the ground and thus require more gravity compensation that resulted in higher shear loading as indicated in **Figure** 3.7(b). As a result, the compression is a more dominant factor to the lower vertebrae while the shearing is more significant to the higher ones during full spine flexion.

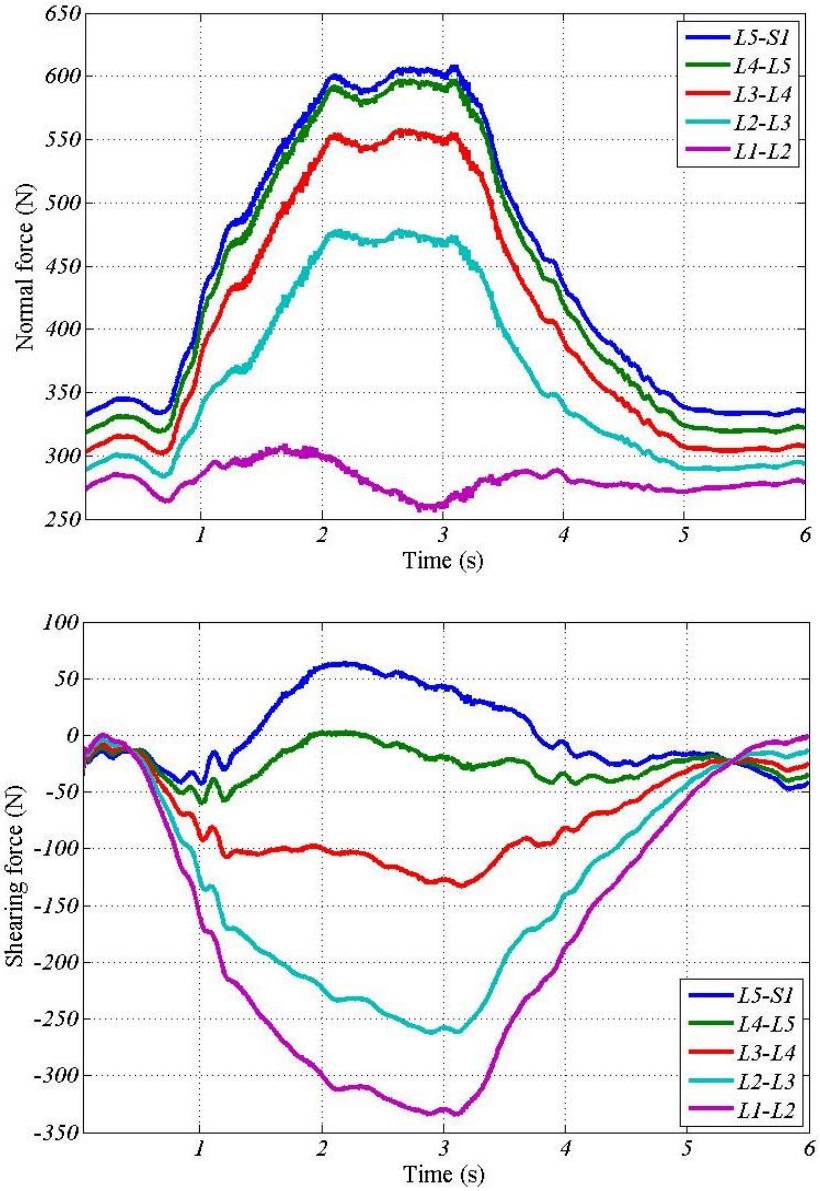

Figure 0.7: Computed joint reaction force during flexion/extension in simulation (a) compression; and (b) shearing

In conclusion, this Chapter introduces the simulation tool used to inform the design process. A musculoskeletal model was developed which combined two existing models in OpenSim. It was used to reconstruct a specific sagittal plane spine flexion/extension in laboratory and was evaluated by comparison to the literature. This model is used as the computational object

for the design phase and the biomechanics results obtained in this chapter are applied as the design reference.

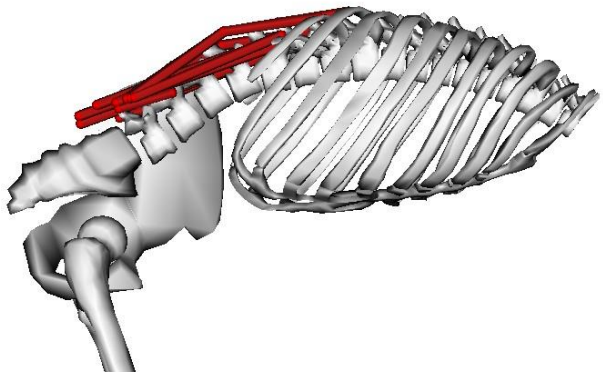

Figure 0.8: Configuration of full spine flexion/extension in the OpenSim

CHAPTER 4

A "PUSH-PULL" EXTERNAL ASSIST STRATEGY FOR THE HUMAN TORSO

Abstract – An OpenSim musculoskeletal model is developed using a simplified multi-link model with only sagittal plane movement. Using this model, a "push-pull" strategy was evaluated to provide external assistance in the sagittal plane for spine flexion/extension. The external assistance was provided by two elastic elements to apply pushing and pulling forces on the lumbar and thorax, respectively, of the human torso in order to decrease muscular effort and to decrease intervertebral reaction torques between the vertebrae in the lumbar region. Simulations results are presented for different spring combinations that individually increment the spring constants.

4.1 The "Push-Pull" External Assist Strategy

The mathematical model was designed as described and is shown in **Figure** 4.1, where the skeleton bodies are drawn by black solid lines and the muscles located on the torso as red. The model consists of multiple links representing the skeleton referred to in similar prior studies [12], [29]. Specifically, the model uses pin joints at the ankle and hip and uses a single flexible rod representing the lumbar vertebrae with two fixed connections with the pelvis and torso.

During human spine flexion, the back muscles stretch and provide pulling forces on the spine. To compensate the muscle power deficiency, an external pulling force can be thereby applied on the back side of thorax paralleling to the back muscles during the motion. This pulling force would generate an additional extensional torque and compression on the lumbar joints, which potentially compromises lumbar stability during the motion. An external pushing force on lumbar from back side can provide necessary supports to eliminate such instability issues. Spring forces were selected to provide such assistance for the consideration of safety and energy conservation

[30], [31]. Two spring forces were added in the model, "**Thorax Spring (TS)**" labeled with blue lines and "**Lumbar Spring (LS)**"labeled with an array of green arrows.

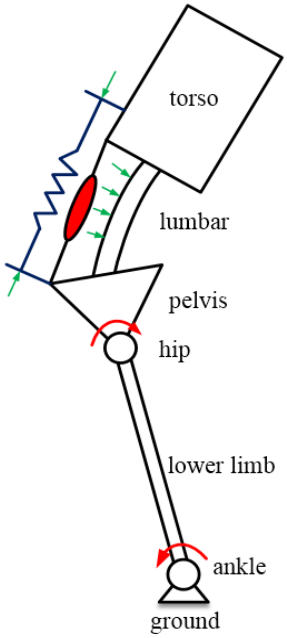

Figure 0.1: Mathematical model of "push-pull" external assist strategy

In **Chapter** 3, biomechanics simulations were developed to reconstruct and visualize the spine flexion/extension in software. Based on the outcomes of these simulations, several assumptions are applied to simplify the model. (1) No motion of either foot relative to the ground, meaning both feet are welded to the ground. (2) Although motion was not perfectly symmetric, it can be considered as a simple two-dimensional flexion/extension in the sagittal plane. (3) The knee joints are locked during the movement, allowing the thigh and shank to be modeled as a single link. (4) The motions of the vertebrae in lumbar section are coupled and thus can be generalized as a single flexible rod. (5) The groups of dorsal muscles used in biomechanics simulations can be simplified into two groups: thorax muscle connecting torso with pelvis and lumbar muscle linking lumbar with pelvis.

4.2 Validation via Biomechanics Simulation

A set of biomechanics simulations were designed in order to illustrate the effects of the "push-pull" strategy. A simulation model in the OpenSim was established using two spring forces, Thorax Spring and Lumbar Spring. Additional geometric features were needed to apply the spring forces in simulation, illustrated in **Figure** 4.2. The Thorax Spring was placed between two welded bodies, shown as green and purple cylinders on torso and pelvis respectively, to apply the pulling force on the torso. The Lumbar Spring was placed between the three consecutive yellow cylinders and the lumbar vertebrae to push the lower back. The cam is a pin joint on the pelvis and its movement is coupled to hip flexion. The springs are not loaded in the fully extended position and the neutral length of the TS is $l_{it} = 0.200$ m and $l_{il} = 0.124$ m for the hip spring.

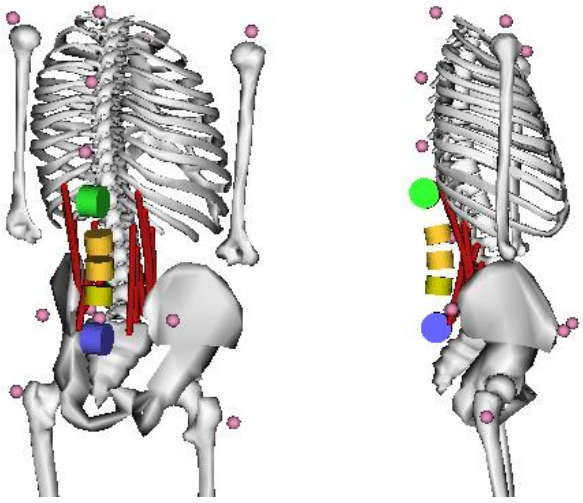

Figure 0.2: "Push-pull" implementation using biomechanics model in OpenSim

The model enables study of the individual influence of each spring by setting different spring constants for each. Initially, the spring constant of Lumbar Spring was set to be 0 and of Thorax Spring was set to values ranging from 0 N/m to 9000 N/m to observe the effect of the Thorax Spring in the forward simulations. The CMC and the joint reaction analyses in the

OpenSim were then repeated to compute the muscle actuation forces and joint reactions in lumbar joints with each different Thorax Spring constant.

The results in **Figure**4.3 show the peak activation force of the total back muscles from the computation decreased with increasing values of Thorax Spring. Also, muscle activation times are remarkably reduced with a larger Thorax Spring constants, which can be inferred from that the muscles postpone activation and finishe it earlier. The reduction in muscle force is not as noticeable for Thorax Spring constants greater than 6000 N/m. As the Thorax Spring constant increases, the intervertebral reaction torque at L_5-S_1 level, shown in **Figure** 4.4, declines on the positive phase and increases the absolute values on the negative phase. This indicates that the Thorax Spring provides a positive assistance in terms of reducing muscle efforts and flexion intervertebral torque. However, it also increases the extension torque that would cause lumbar instability.

Then, the Lumbar Spring constant is increased from 0 to 3000 N/m so that an increasing pushing force was applied on the lumbar, shown in **Figure** 4.5. The intervertebral reaction torques move up with the increment of the Lumbar Spring constant. Contrary to the Thorax Spring, the Lumbar Spring increases the flexion intervertebral torque while decreasing the extension intervertebral torque. In addition, the muscular effort does not show much difference with different pushing force from Lumbar Spring, as indicated in **Figure** 4.6.

With the "push-pull" strategy, the profiles of the intervertebral reaction force are modified. **Figure** 4.7 illustrates under the pulling force and pushing force, the lumbar reacts more compression and shearing. Studies introduced in [1] indicated the maximum reaction forces that the average population throughout all age can bear was 2 KN for compression and 600 N for shearing, respectively. Hence the maximum reaction forces with "push-pull", compression 1 KN and shearing 300 N, shown in **Figure** 4.7 are still in the safety ranges. These increments of reaction

forces are also believed to be much smaller in reality due to more completed structures in human body introduced in last chapter.

In conclusion, the "push" and "pull" is more assistive when coupled. The paralleled muscle-like pulling force on the torso from pelvis mainly increases the muscle capability while the pushing force coupled with hip flexion stabilizes the flexible lumbar and thereby lowers the intervertebral torques. To design an exoskeleton to embody this strategy, the design parameters should be optimized of this external assistance to the torso.

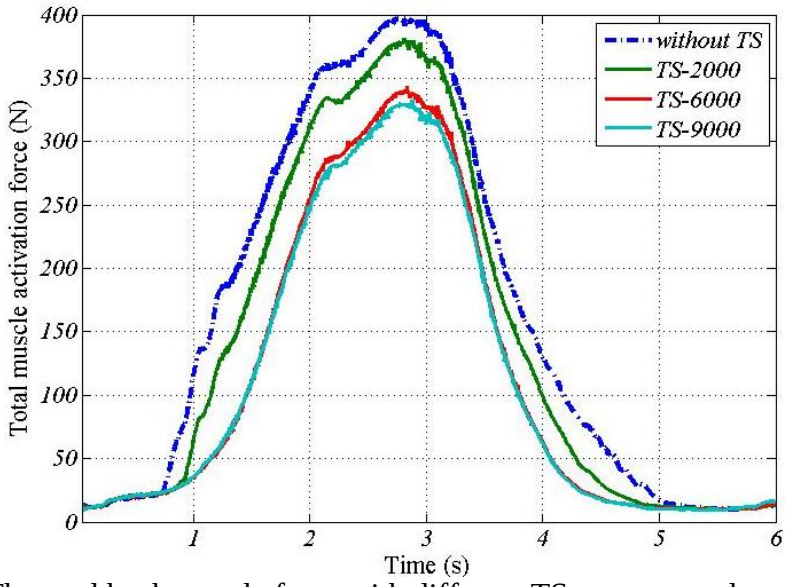

Figure 0.3: The total back muscle force with different TS constant and zero LS constant

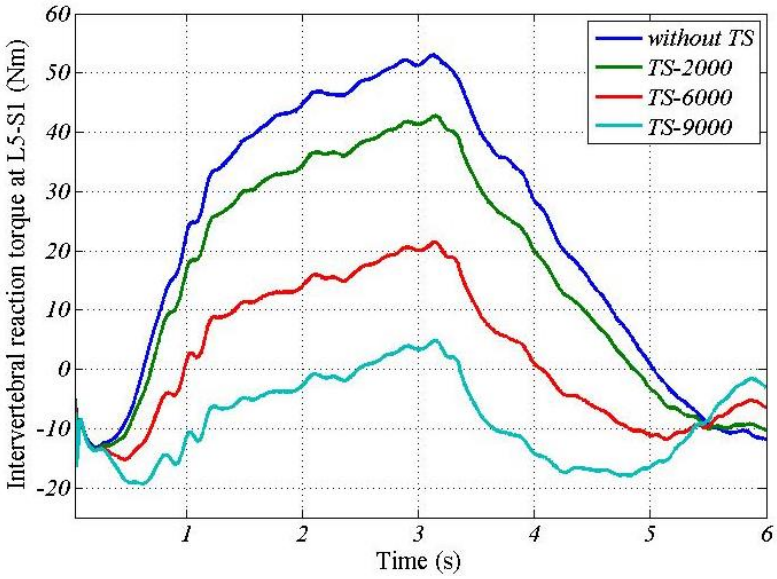

Figure 0.4: The intervertebral torques at L5-S1 level with distinct Thorax Spring constants and zero Lumbar Spring constant

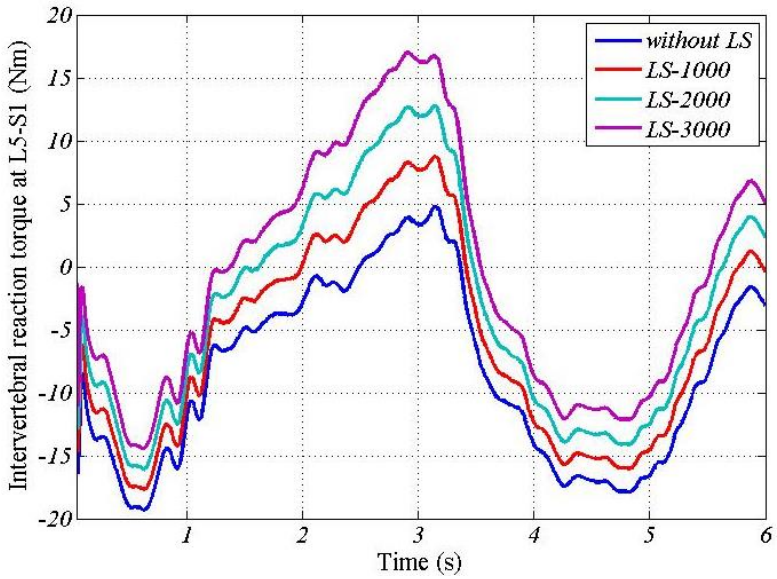

Figure 0.5: The intervertebral reaction torques in lumbar at L_5-S_1 with identical Thorax Spring constant (6000 N/m) and distinct Lumbar Spring constants

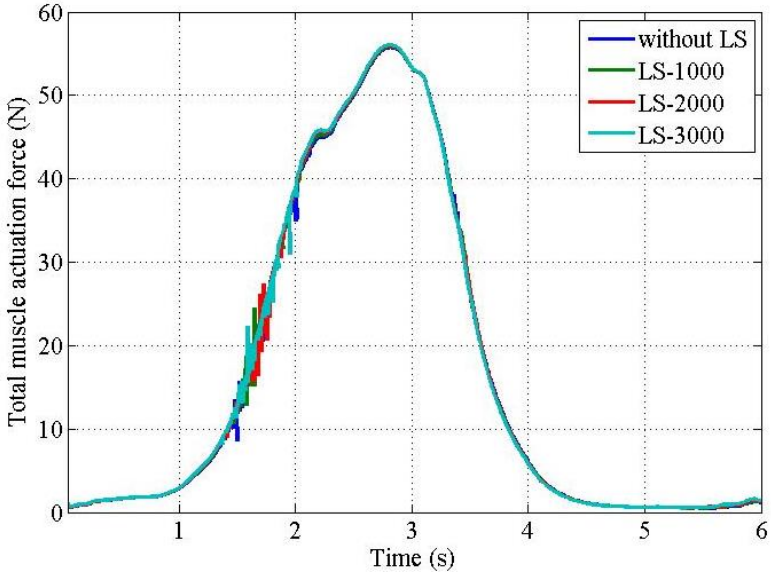

Figure 0.6: The total muscle activation forces with identical Thorax Spring constant (6000 N/m) and different Lumbar Spring constants

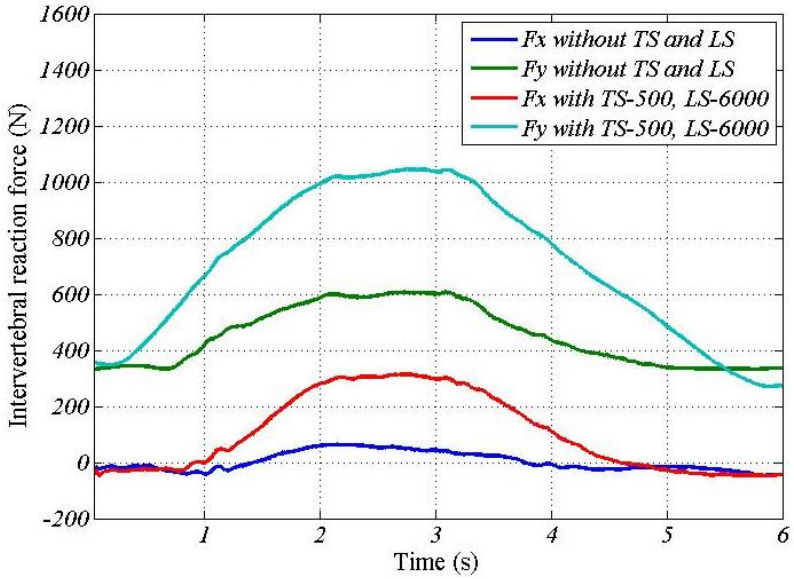

Figure 0.7: The compression (Fy) and shearing (Fx) reaction forces without Thorax Spring and Lumbar Spring comparing with the ones with Thorax Spring and Lumbar Spring

CHAPTER 5

OPTIMIZATION OF THE ELASTIC ELEMENTS IN THE "PUSH-PULL" ASSISTIVE STRATEGY

Abstract – In this chapter, the spring constants for the "push-pull" assistive strategy are optimized to minimize muscular efforts and intervertebral torques and forces of the operator. Since it is a multiple objective optimization problem, a Monte Carlo approach is employed to search for the global optimal solution. To iteratively update the design parameters Matlab scripting is used to run the OpenSim simulations. The optimal result is presented and discussed.

5.1 Optimizing the "Push-Pull" Strategy

Linear springs are defined by their spring constants which needs to be selected. The spring constant fully describes the force-displacement relationship of the spring according to ***Hooke's Law***. The two objectives of this optimization are minimizing the back muscle efforts and the intervertebral reaction torques. In this study, the **Back Muscle Effort** was defined as the mean value of the summation of all back muscle forces listed in **Table** 3.1, and the **Intervertebral Reaction Torque** was indicated by the mean of the maximum absolute intervertebral reaction torque at each lumbar level during the entire spine flexion/extension. It is a multiple objective optimization problem of seeking for an optimal combination of pushing and pulling forces (spring constants) of the external assistive strategy.

The criteria of the optimization could be expressed mathematically as,

$$\textbf{Minimize} \qquad \boldsymbol{g(k)} = \left\| \begin{bmatrix} \sum \overline{F_m/F_{m0}} \\ \max M_z/M_{z0} \end{bmatrix} \right\| \tag{0-1}$$

$$\textbf{Subject to} \qquad \boldsymbol{lb} \leq \boldsymbol{k} \leq \boldsymbol{ub},$$

where,

$$\boldsymbol{k} = \begin{bmatrix} k_T \\ k_L \end{bmatrix}, \boldsymbol{lb} = \begin{bmatrix} 2500 \\ 200 \end{bmatrix}, \boldsymbol{ub} = \begin{bmatrix} 9000 \\ 2000 \end{bmatrix}.$$

Here is using 1-norm to weight the two objectives in the cost function $\boldsymbol{g}(\boldsymbol{k})$ since there is no preference to our interest. The objectives are normalized by the corresponding maximum value from the natural body simulation results illustrated in **Figure** 3.5 and 3.6 since the force and torque are different physics variables. The objectives relate the spring constants nonlinearly with the biomechanics computation processes in OpenSim (the CMC and the Joint Reaction Analyses). Of the spring constants, k_T represents for the spring constant of the pulling force while k_L is the spring constant of the pushing force. The searching range of the spring constants are constrained with lower ($\boldsymbol{lb}$) and upper bounds ($\boldsymbol{ub}$).

5.2 Optimization by Monte Carlo via Matlab Scripting and OpenSim Simulation

5.2.1 Simulation Set Up

OpenSim was employed to compute the muscle activation forces and joint reactions with different spring constants, iteratively. Besides the user interface provided by OpenSim to manually modify models and simulation parameters, it also provides the ability to script the simulations outside OpenSim via other programming platforms such as Matlab. **Figure** 5.1 shows the flow of this approach. The scripting starts with the initialization of the design parameters, then it accesses OpenSim to iteratively run the biomechanics simulations with the Monte Carlo approach, then it saves the results, and finally returns the optimal result from the full result set.

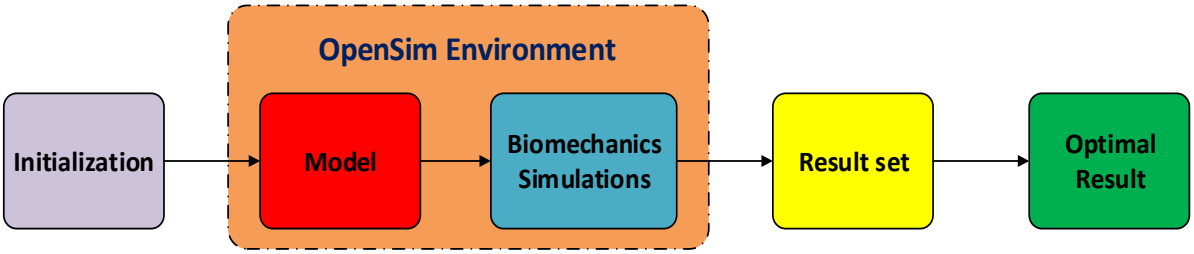

Figure 0.1: Flowchart of optimization via Matlab scripting OpenSim simulations

For the computational consideration each simulation run time was about 25 minutes on a regular desktop PC, Processor@2.80 GHz, RAM 9 GB. The simulations were operated for 250 times by applying the Monte Carlo approach to explore the system variations in the specific search range.

5.2.2 Optimization Results

The plots in the **Figure** 5.2 and 5.3 present a surface fitting of the simulation results with actual points marked by the black stars. The results illustrate that the Back Muscle Effort decreases dramatically with the Thorax spring constant rising. In addition, the rate of change becomes slower when the Thorax Spring constant is below 6000 N/m. There exists an obvious valley from the Intervertebral Reaction Torque result, which ranges from 6000 – 9000 N/m for the Thorax Spring constant and 200 – 2000 N/m for the Hip Spring constant. It represents the optimal result with respect to the Intervertebral Reaction Torque. By applying no preference weights for the two objectives, the global optimal solution $\boldsymbol{k_{opt}}$ was found and is shown in **Figure** 5.4.

$$\boldsymbol{k_{opt}} = \begin{bmatrix} k_T \\ k_L \end{bmatrix} = \begin{bmatrix} 8594 \\ 1921 \end{bmatrix} (N/m).$$

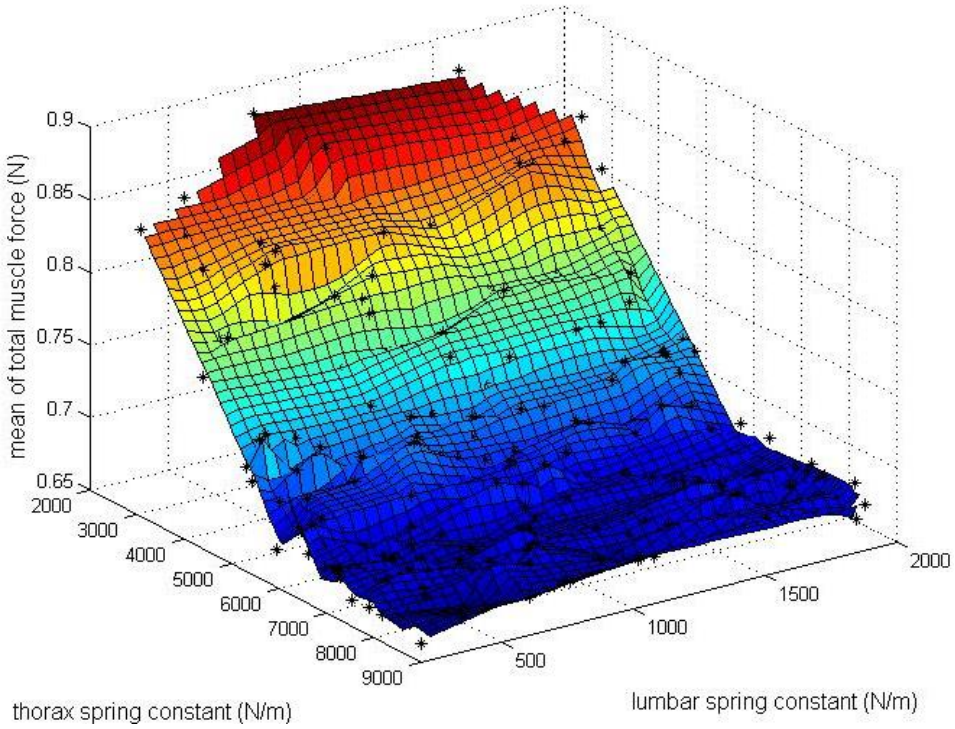

Figure 0.2: The relationship between the Back Muscle Effort and the spring constants

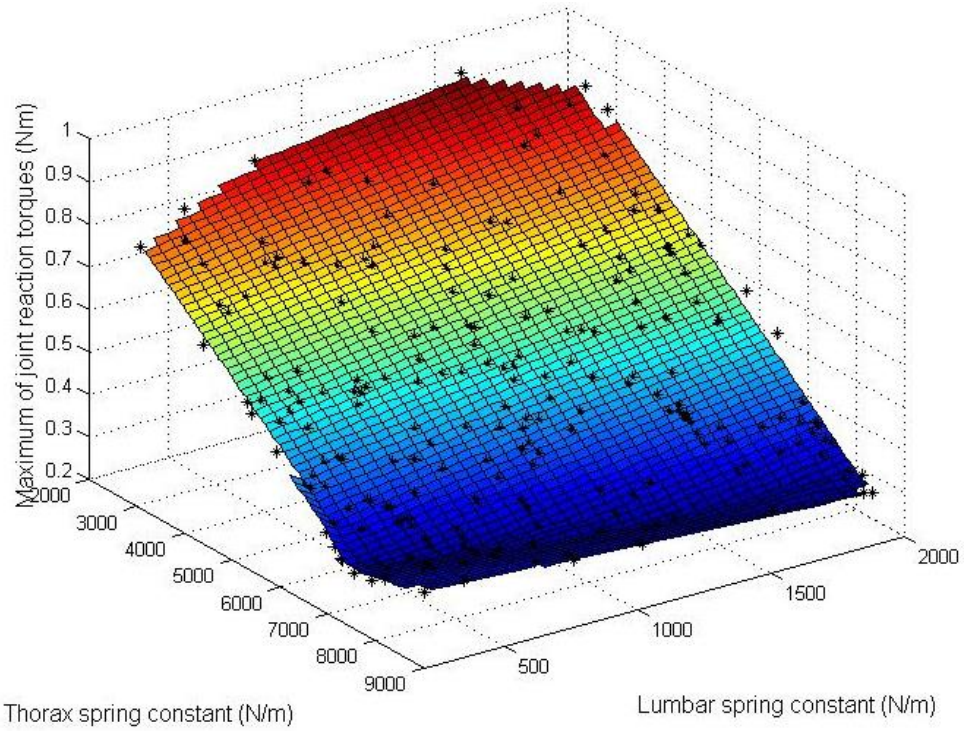

Figure 0.3: The relationship between the Intervertebral Reaction Torque and the spring constants

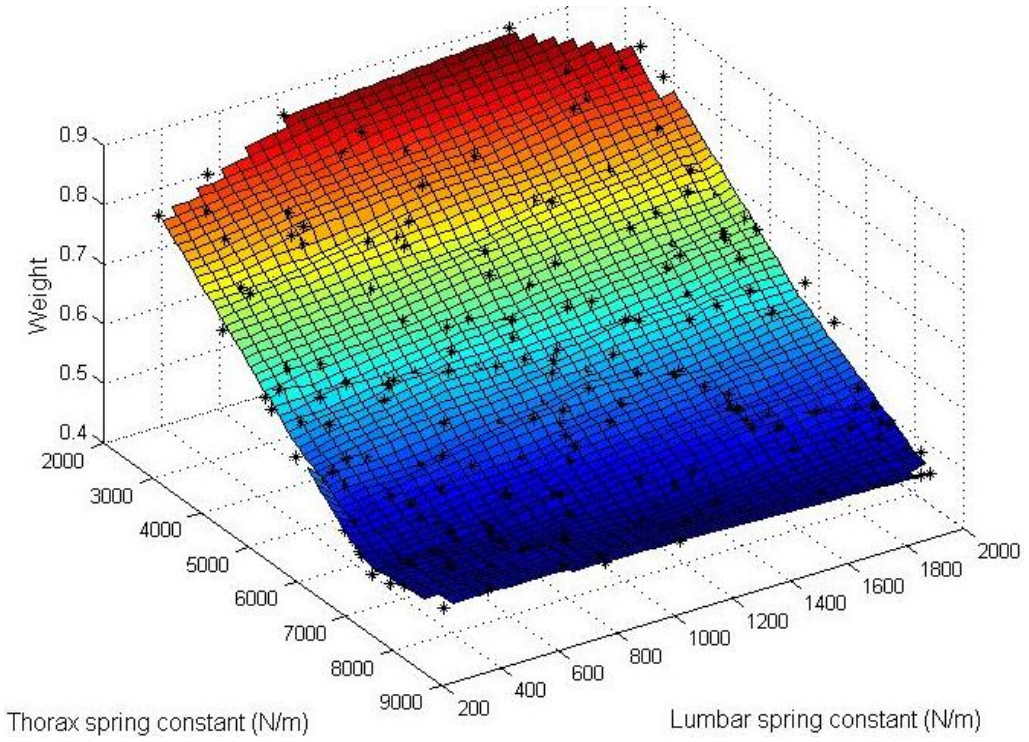

Figure 0.4: The weight plot for seeking the optimal spring constants

5.3 Result Estimation and Analysis

Figure 5.5 and 5.6 show the final results of the optimal exoskeleton spine in terms of the Back Muscle Effort and the Intervertebral Reaction Torque. It indicates a 16% (65 N) peak reduction and a 31% mean reduction with respect to the Back Muscle Effort, while a 71% peak reduction (37 Nm) and 78% mean reduction with respect to the Intervertebral Reaction Torque.

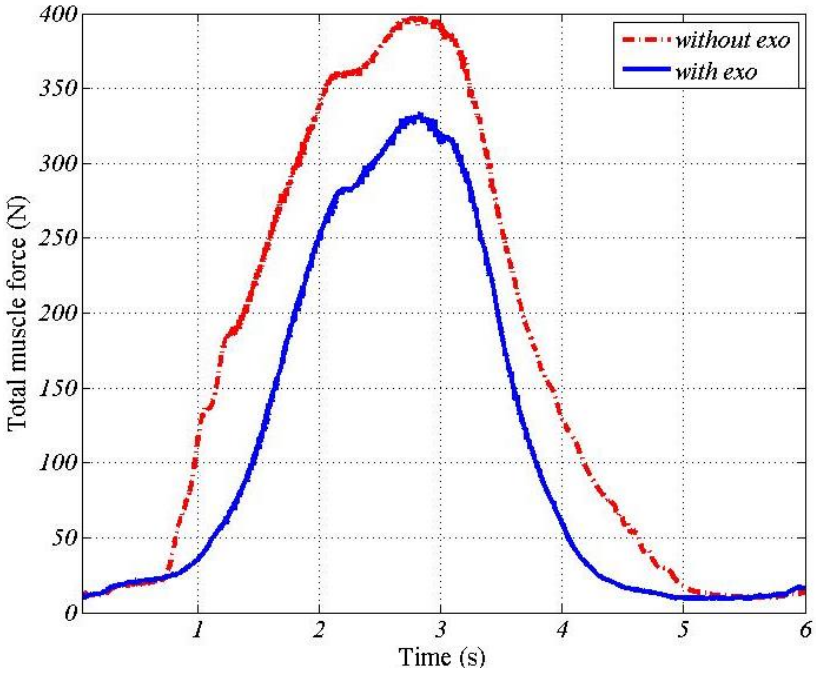

Figure 0.5: The comparison of the computed total muscle activation force between with the optimal spring constants and the natural body

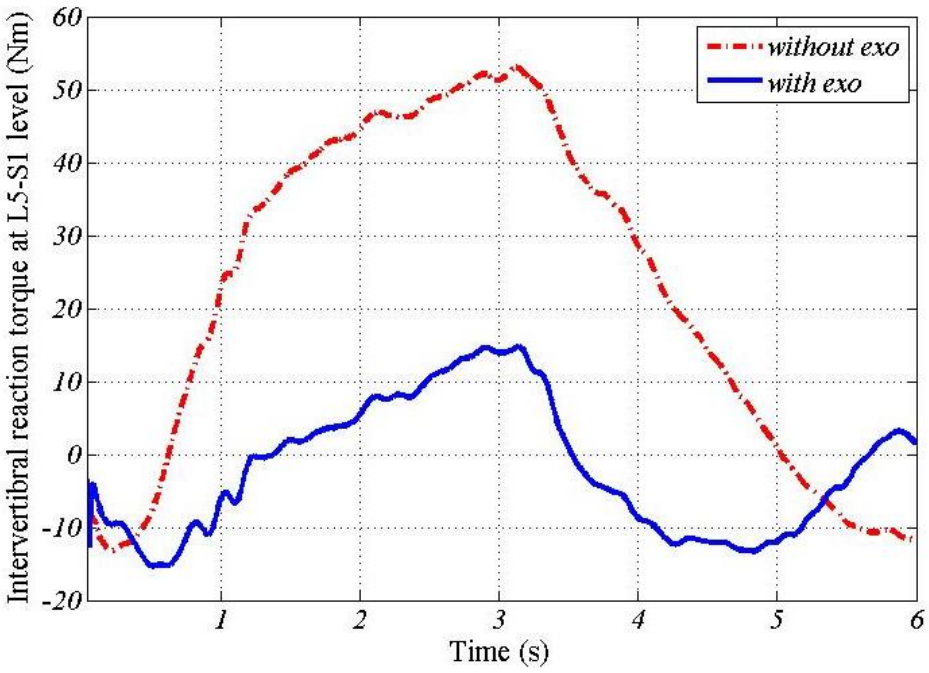

Figure 0.6: The comparison of the computed intervertebral torque at L_5-S_1 lumbar level between with the optimal spring constants and the natural body

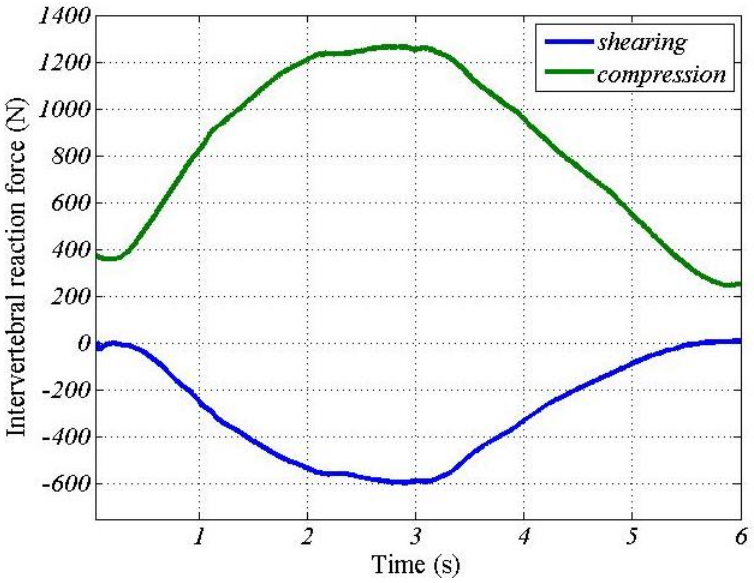

Figure 0.7: The maximum reaction forces (compression at L_5-S_1, shearing at L_1-L_2) in lumbar with the optimal spring forces

In addition, **Figure** 5.7 shows the largest intervertebral forces in the lumbar, where the maximum compression occurred at L_5-S_1 level and the maximum shearing at L_1-L_2 level. Comparing the assisted results with the computational reaction forces results with the unassisted spine introduced in **Chapter** 3, the maximum compression and shearing both double, but they are still within the safety range introduced from relative studies in [1]. Recall that the model does not include features resisting the shearing force in reality such as intra-abdominal pressure and facet joints as mentioned in **Chapter** 3, the reaction forces occurs at the discs would be much lower in reality.

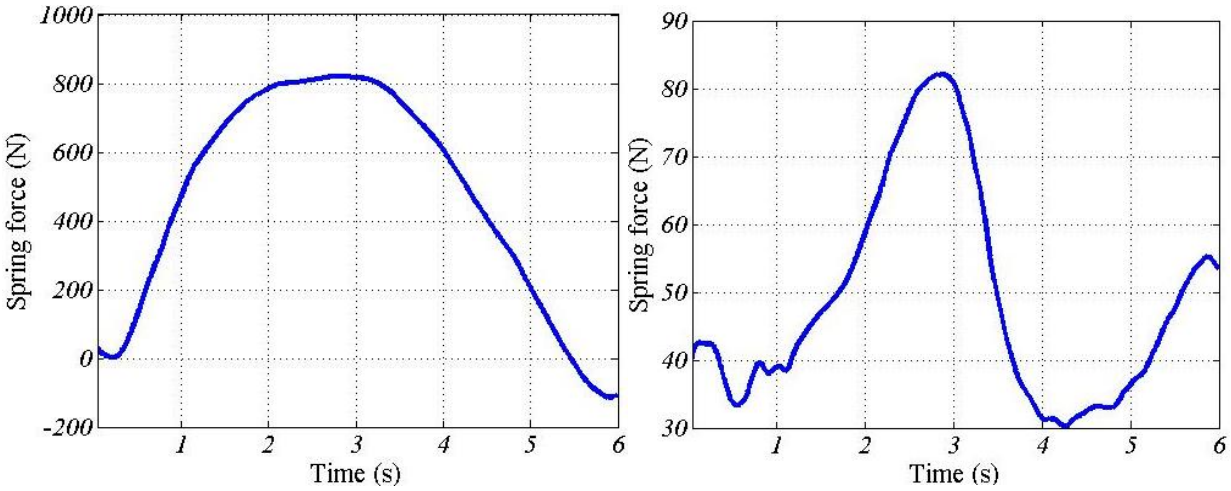

Figure 0.8: The optimal spring forces: (a) the pulling force, and (b) the pushing force

Figure 5.8 shows the spring forces generated during flexion/extension of the torso with the optimal spring constants outputted by the simulations. The peak pulling force reaches around 800 N while the pushing force varies between 30 to 83 N. These two spring forces were correlated with the Back Muscle Effort and the Intervertebral Reaction Torque reduction to further discuss how the contribution of each spring individually. **Table** 5.1 lists the correlation coefficients between each two variables. Plus, **Figure** 5.9 illustrates the mapping between the reduction of each objective and the individual spring force at each time point during torso flexion and extension.

Table 0.1: Correlation coefficients between the spring forces and the Back Muscle Effort and the Intervertebral Reaction Torque reductions

	Back Muscle Effort reduction	Intervertebral Reaction Torque reduction
Pulling force by TS	0.71	0.90
Pushing force by LS	0.14	0.63

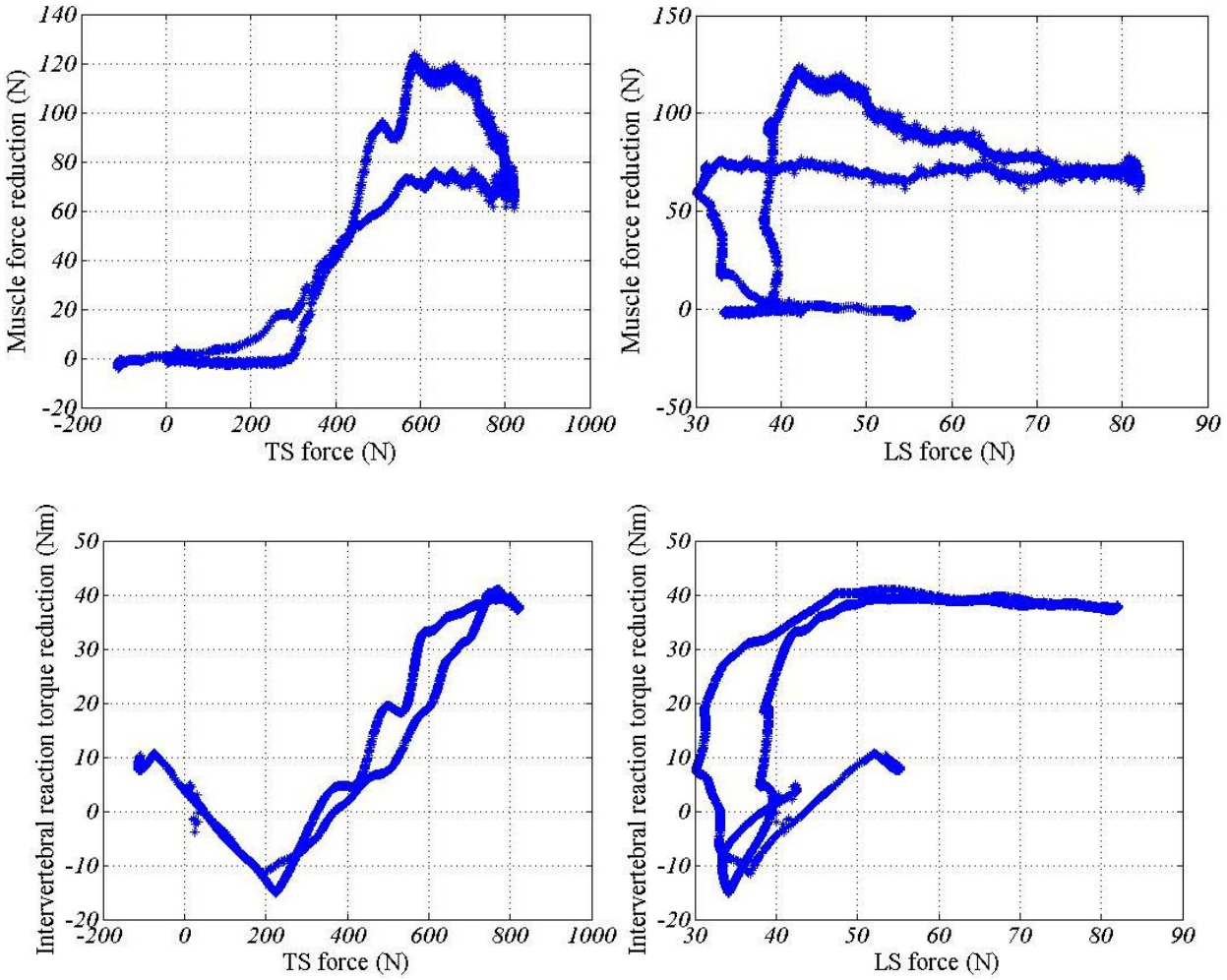

Figure 0.9: Relationships between each objective reduction and individual spring force

It indicates the Thorax Spring pulling force primarily contributes to the muscle effort reduction and the intervertebral torque. Even though the Lumbar Spring pushing force contributes little in terms of the Back Muscle Effort, it provides considerable influence on the Intervertebral Reaction Torque reduction. Especially when considering the much smaller magnitude of the pushing force compared to the pulling force. The contribution by the Lumbar Spring is significant because it compensates the excessive extensional torque provided by the Thorax Spring.

In summary, this chapter details a method to optimize design parameters using Matlab scripting to run the OpenSim simulations. The optimal spring constants found can reduce the Back

Muscle Effort and Intervertebral Reaction Torque in biomechanics simulations. These results were used to guide the mechanism design and prototype implementation in the remaining chapters.

CHAPTER 6

REALIZING THE "PUSH-PULL" ASSISTIVE STRATEGY

Abstract – Due to the inevitable differences between the simulation and the physical implementation, a physical prototype was designed and constructed to evaluate the "push-pull" assistive strategy and simulation. A passive spine exoskeleton was designed to satisfy the specific requirements of the "push-pull" strategy and the significant parameters were converted from the simulation to the implementation through the mechanical design.

6.1 Physical Modeling

A detailed physical model was created according to the "push-pull" strategy, whose 3D model is illustrated in **Figure** 6.1. The model consists of three major sections worn by the operator: a pelvic cuff is attached to the waist of the operator; a shoulder harness; two thigh cuffs with two foot straps that loop under the feet and used to connect the thigh cuff with the pelvic cuff. Extension springs connect these three sections to realize the push and pull forces. The lumbar spring is parallel to the spine and links the pelvic cuff with the shoulder belt. The hip spring is connected to rotate cam mounted on the pelvic cuff via a cable-tension mechanism and then connects to the thigh cuffs on each side. The cams are pin jointed on the pelvic cuff and therefore has only one degree of freedom to rotate about the transverse axis. As a result, hip rotation causes the cam to rotate which then pushes on the operator's lumber region. Lastly, foot straps were mounted to connect the hip and pelvic cuffs to the feet to resist the force of the lumber spring during torso flexion.

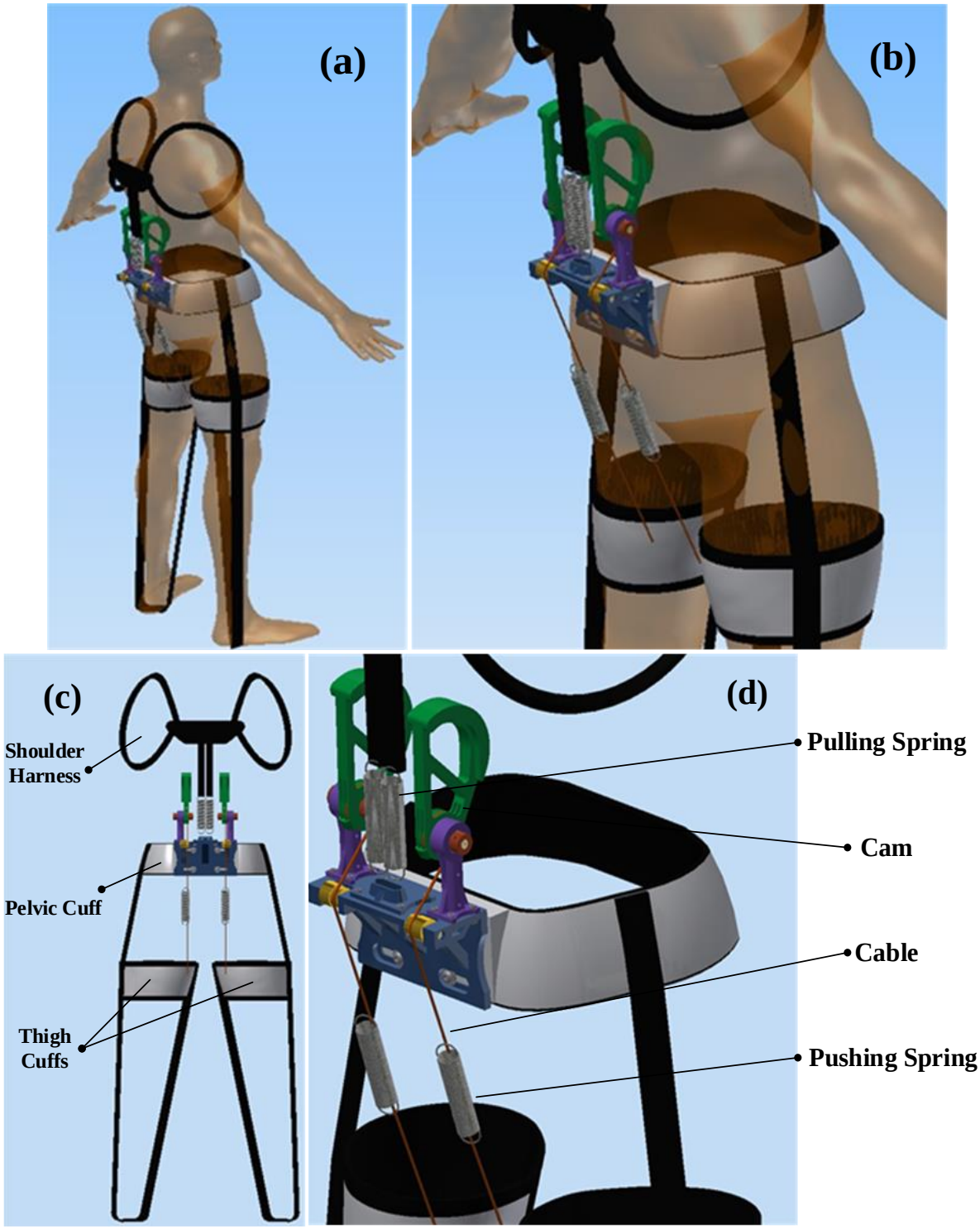

Figure 0.1: 3D physical model for passive exoskeleton spine suit: (a) view of wearing on user; (b) view zoomed in of wearing on user; (c) back view of the suit; (d) mechanism details.

6.2 Prototype Fabrication

A prototype was fabricated to evaluate the "push-pull" strategy using the physical model and the optimal spring constants from the optimization. Also from the simulation results, the full set of spring parameters were defined, such as the deformation, the maximum load capacity and the physical size. Key parameters are listed in **Table** 6.1.

Table 0.1: Optimized spring constant in biomechanics simulation

	Maximum deformation (m)	Maximum force (N)	Spring constant (N/m)	Rest length (m)
Thorax Spring	0.095	820	8594	0.200
Lumbar Spring	0.043	83	1921	0.124

The Thorax Spring selection for prototype was more straightforward due to the alignment of the prototype and simulation models. The Lumbar Spring selection was more difficult because the Lumbar Spring is set between the cam and the lumbar in the simulation and is nearly impossible to implement a safe and measurable spring force following hip movement in reality. Instead, a cable tension mechanism was used. The extension spring in the tension mechanism needed to be selected according to the mathematical modeling of the mechanism, indicated in **Figure** 6.2. The two identical mechanisms are placed on either side of the spine. The output was the virtual pushing force F_L provided by the Lumbar Spring from the simulation, while the input was the real spring force T. In this mechanical system, the torque offered by the input and output should be identical if the inertial effects of the cam can be neglected, which therefore was,

$$T \cdot r = k_L \cdot \Delta l_L \cdot r_L \tag{0-1}$$

Where the r and r_L can be measured from the physical model. In addition, either the virtual spring force or the spring force in reality obeyed the ***Hooke's Law*** that $T = k_h \cdot \Delta l_h$ and $F_T = k_L \cdot \Delta l_L$. Plus, the displacement Δl_L and Δl_h can be obtained from the simulation and model geometry.

Therefore, the pushing spring constant can be defined. Since there are two extension springs on either side of the spine, the spring constant should be half of k_h. The final springs selected for the physical prototype are shown in **Table** 6.2.

Table 0.2: Specification of the extension springs applied in the prototype

	Rest length (m)	Spring constant (N/m)	Outer diameter (m)	Extended Lg. (m)
Pulling Spring	0.105	6700	0.015	0.240
Pushing Spring	0.050	2000	0.012	0.120

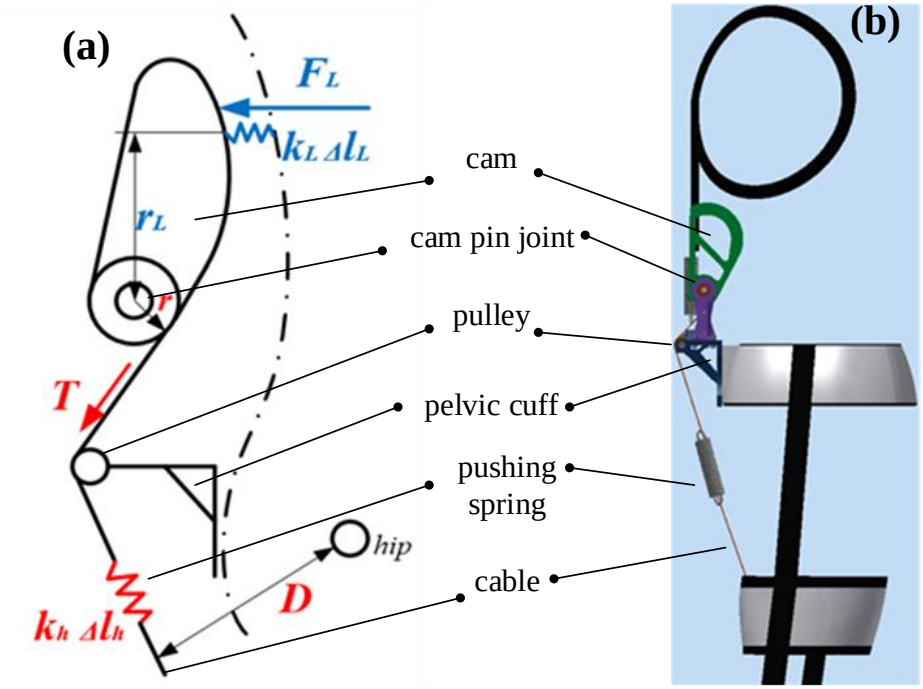

Figure 0.2: The cable-tendon mechanism of applying the pushing spring force on the human back: (a) mechanism sketch; (b) side view of 3D model.

The physical model was then fabricated and assembled. Most parts consisted of the structure were 3D printed in ABS plastic. The posts for holding rotational joints of the cams (shown in purple color in 3D models) were printed hollow while inserted with a steel shaft to strengthen the structure besides the ribs and intersection shape design of the part. The rotational joints were supported by the ball bearings. Buckles were used to adjust the prototype and tension the cables.

CHAPTER 7

PROTOTYPE EVALUATION

Abstract – The prototype was evaluated on human subjects. Three subjects were asked to complete both dynamic and static sagittal plane flexion/extension tasks with and without wearing the exoskeleton device. The sEMG and inertial data were collected in both conditions on the certain levels of the dorsal muscles for each subject. The experimental setup and the signal post-processing are presented in detail. The effects of the prototype are evaluated by comparing the patterns and magnitudes of the signals collected under both conditions.

7.1 Experiment Setup

This experiment involved three human participants and was approved by the University of Massachusetts – IRB. The subject physical properties were listed in **Table** 7.1. Eight electrodes (10 mm spacing; Ag-AgCl) from a sixteen-channel Delsys wireless sEMG system sampled at 2.0 kHz were placed on posterior of the subject's torso to record dorsal muscle excitations, shown in **Figure** 7.1. To match with the musculoskeletal model constructed in OpenSim, the erector spinae excitations at L_3, L_1, T_{11} and T_{10} levels (from bottom to top) were specifically captured with and without the exoskeleton. Since the EMG sensors on L_1 and T_{10} level interfered with the interaction between the exoskeleton and human lower back, these four channels were removed in the tests of the subject wearing the exoskeleton. In addition, an accelerometer is embedded in each EMG sensor and was used to record the three dimensional inertial information during the movement. Inertial sensors were recorded at 1482 Hz. Since the target subject was required to accomplish flexion tasks only in sagittal plane, the inertial data was assumed to be identical from the sensors on both sides at the same vertebra level. Therefore, the inertial outputs were set to be the angle

changes from the left side channels while the linear accelerations from the right side channels. Therefore, both linear and angular inertial information was obtained simultaneously.

Table 0.1: Subject physical properties

	Subject No.1	Subject No.2	Subject No.3
Weight (kg)	63	75	67
Height (m)	1.65	1.84	1.67
Age (year)	25	25	30

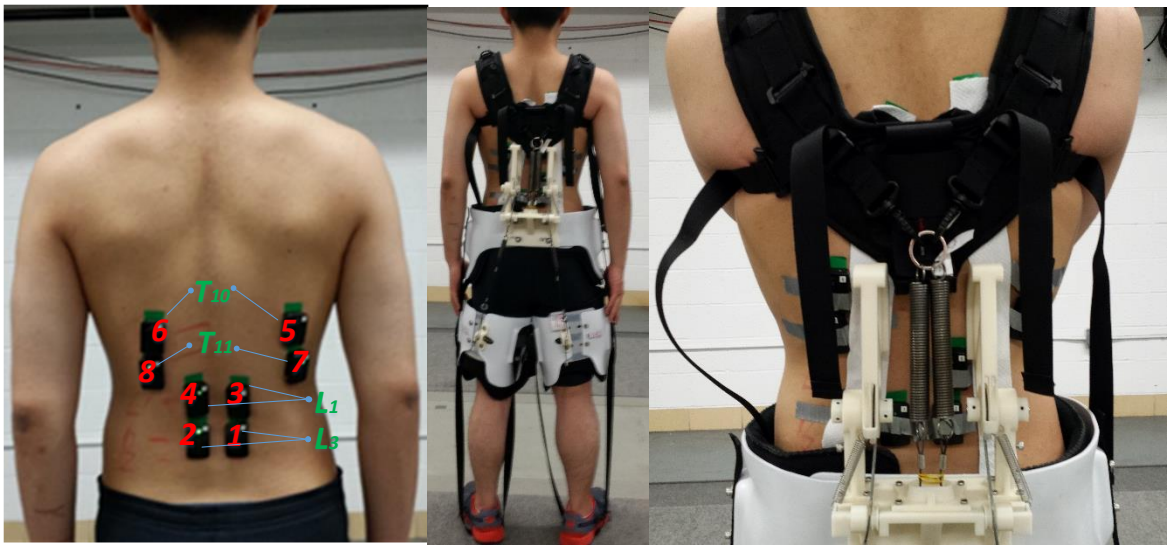

Figure 0.1: (a) EMG sensor distributions on the back of subject; (b) and (c) configurations of the subject wearing the exoskeleton spine prototype.

The tests conducted investigate the performance of the prototype in terms of dynamics and statics. The protocol of the experiment was introduced in **Table** 7.2. During the dynamic test, the subjects were asked to repeat the identical specific sagittal plane spine flexion/extension introduced in the **Chapter** 3. During the static tests, they were required to flex to a certain position (as listed in **Table** 7.2) and stay there for a certain time (as listed in **Table** 7.2) in each trial as shown in **Figure** 7.2. The subject's left shoulder height to the ground was measured to make sure they stayed in the correct position. The spring extensions in different trials were recorded. Additionally, the subjects rested after every other trial for 3 minutes. The subjects were tested

without the exoskeleton before the test wearing the exoskeleton, which obtained accurate results from the natural body and avoid giving advantage to the exoskeleton spine.

Table 0.2: Experiment Tasks List

Dynamic Test without Exoskeleton: Flexion/Extension – Bend forward and stand back up – 60 bpm – 20 times – 120s			
Static Test without Exoskeleton:	Subject No. 1	Subject No. 2	Subject No. 3
(1) Static Flexion – Position 1	1220 mm, 120 s	1450 mm, 90 s	1220 mm, 90 s
(2) Static Flexion – Position 2	1070 mm, 120 s	1340 mm, 90 s	1100 mm, 90 s
(3) Static Flexion – Position 3	950 mm, 120 s	980 mm, 90 s	1000 mm, 90 s
Repeat the above tests wearing with Exoskeleton			

As was shown, the cams of the exoskeleton contact the human back during the operation. In this case, some sensors had to be removed due to the spacing conflicts between the sensor and this human-machine interaction. The sensor remained were slightly different for different subjects, which are specified in **Table** 7.3.

Table 0.3: Sensor number remained during tests wearing exoskeleton for different subjects

	Subject No. 1	Subject No. 2	Subject No. 3
Channel Remained	Ch.1: right L_3 Ch. 2: left L_3 Ch. 7: right T_{11} Ch. 8: left T_{11}	Ch.2: right L_3 Ch. 4: right L_1 Ch. 7: right T_{11} Ch. 8: left T_{11}	Ch.2: right L_3 Ch. 4: right L_1 Ch. 7: right T_{11} Ch. 8: left T_{11}

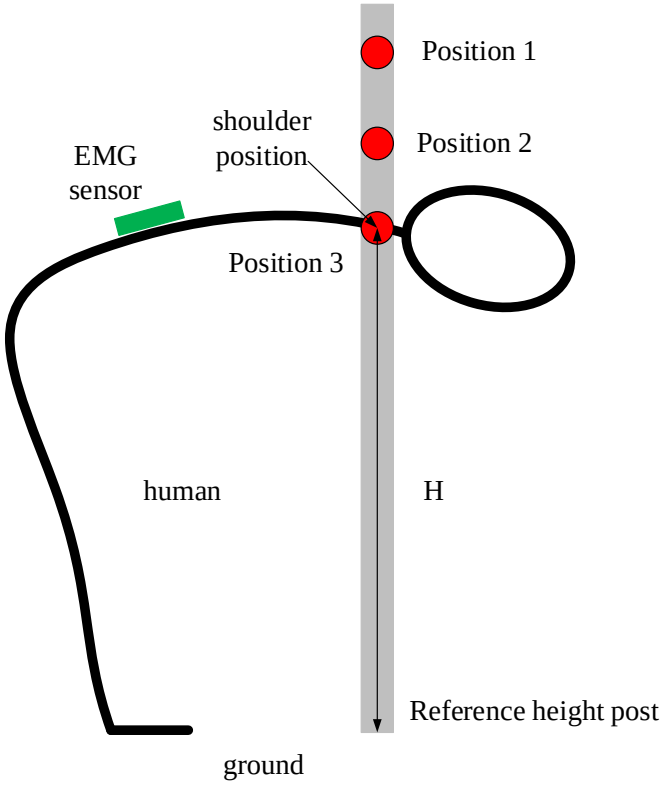

Figure 0.2: Static test setup

7.2 Dynamic Evaluation

Figure 7.3 illustrates the dynamics during sagittal plane spine flexion/extension of a subject. The green block represents the EMG sensor, whose coordinate system is indicated in **Figure** 7.3. Assuming that the muscle forces at the sensor attachment point are tangent to the human torso and the mass of the exoskeleton and sensors can be neglected compared to the mass of the human torso, the dynamic equations can be obtained as following:

Without exoskeleton,

$$\begin{cases} \sum \boldsymbol{F_x} = m\boldsymbol{a_x} = -\boldsymbol{G}\cos\boldsymbol{\theta} - \boldsymbol{F_M} \\ \sum \boldsymbol{F_z} = m\boldsymbol{a_z} = -\boldsymbol{G}\sin\boldsymbol{\theta} \\ \sum \boldsymbol{M_o} = I\ddot{\boldsymbol{\theta}} = \boldsymbol{G}D - \boldsymbol{F_M}d - \boldsymbol{\tau} \end{cases} \quad (0\text{-}1)$$

With exoskeleton,

$$\begin{cases} \sum \boldsymbol{F_x} = m\boldsymbol{a_x'} = -\boldsymbol{G}\cos\boldsymbol{\theta} - \boldsymbol{F_M'} - \boldsymbol{F_{TS}}\cos\boldsymbol{\alpha} \\ \sum \boldsymbol{F_z} = m\boldsymbol{a_z'} = -\boldsymbol{G}\sin\boldsymbol{\theta} - \boldsymbol{F_{LS}} + \boldsymbol{F_{TS}}\sin\boldsymbol{\alpha} \\ \sum \boldsymbol{M_o} = I\ddot{\boldsymbol{\theta}}' = \boldsymbol{G}D - \boldsymbol{F_M'}d - \boldsymbol{F_{TS}}d_{TS} - \boldsymbol{F_{LS}}d_{LS} - \boldsymbol{\tau}' \end{cases} \quad (0\text{-}2)$$

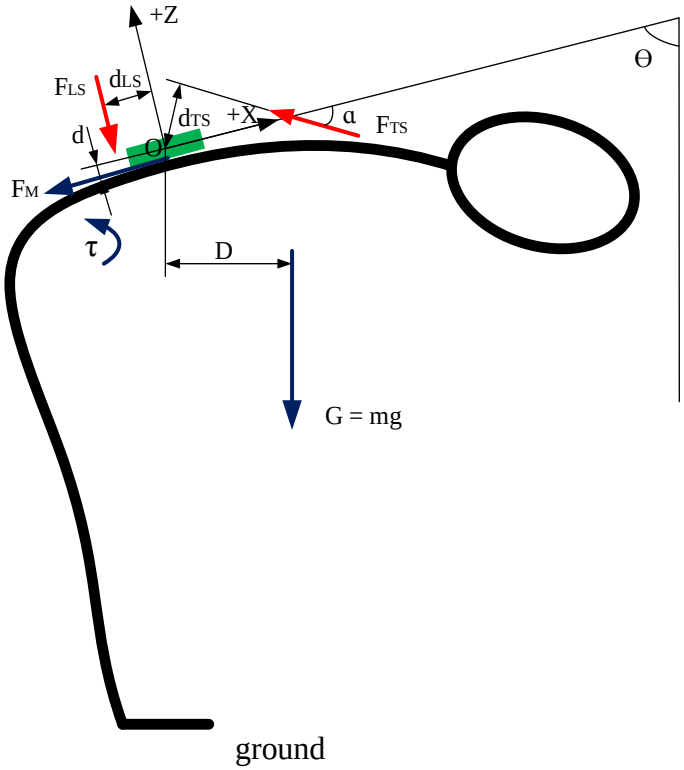

Figure 0.3: Dynamic model for subject flexion with EMG and inertial sensor attached

Subtracting Equation (7-2) from (7-1) gives the equations of motion.

$$\begin{cases} m\Delta\boldsymbol{a_x} = \boldsymbol{F_{TS}}\cos\boldsymbol{\alpha} - \Delta\boldsymbol{F_M} \\ m\Delta\boldsymbol{a_z} = \boldsymbol{F_{LS}} - \boldsymbol{F_{TS}}\sin\boldsymbol{\alpha} \\ I\Delta\ddot{\boldsymbol{\theta}} = \boldsymbol{F_{TS}}d_{TS} + \boldsymbol{F_{LS}}d_{LS} - \Delta\boldsymbol{F_M}d - \Delta\boldsymbol{\tau} \end{cases} \quad (0\text{-}3)$$

In Equation (7-3), m is the mass of the human torso while I is its moment of inertia. The angle $\boldsymbol{\alpha}$ between the TS and the *x* axis of the sensor coordinate can be calculated from the geometry of the exoskeleton and the spring extension. Plus, the moment arms for each force D, d_{TS}, d_{LS} and d can be measured or estimated through the geometry. In addition, the flexion angle $\boldsymbol{\theta}$, the linear

acceleration at the attachment point $\boldsymbol{a_x}$ and $\boldsymbol{a_z}$ can be obtained from the output inertial data from the sensor. The pulling force $\boldsymbol{F_{TS}}$ and pushing force $\boldsymbol{F_{HS}}$ can be computed by the spring constant and the spring extension according to the ***Hooke's Law***. As a result, the muscle force reduction $\Delta \boldsymbol{F_M}$ and $\Delta \boldsymbol{\tau}$ can be estimated.

7.3 Results Comparison for Dynamic Tests

In this section, the data differences between dynamical testing without the exoskeleton and wearing with the exoskeleton are compared. From the dynamic analysis, the inputs to the human spine during flexion/extension are the muscle forces and the spring forces provided by the exoskeleton, while the outputs are the three-dimensional linear accelerations. Since the magnitude of the sEMG signal indicates muscle activation, it was collected along with the linear accelerations simultaneously through each channel of the EMG sensors.

Since the raw sEMG was very noisy, it was post-processed by the following steps: (1) Detrended; (2) high pass filtered at 2 Hz; (3) low pass filtered at 450 Hz; (4) normalized; (5) rectified; and (6) low pass filtered at 3 Hz. It should be mentioned that the signals (channel 1, 2, 7 and 8) used for result comparison were normalized by the maximum value of both with/without exoskeleton tests. **Figure** 7.4 illustrates these processes in order, where the sEMG signal was from channel 1 on the right side at L_3 level of the Subject No. 1 in the dynamic test. The clean signal after the final low-pass filter demonstrated the variations of the rectified signal, which was shown in **Figure** 7.5.

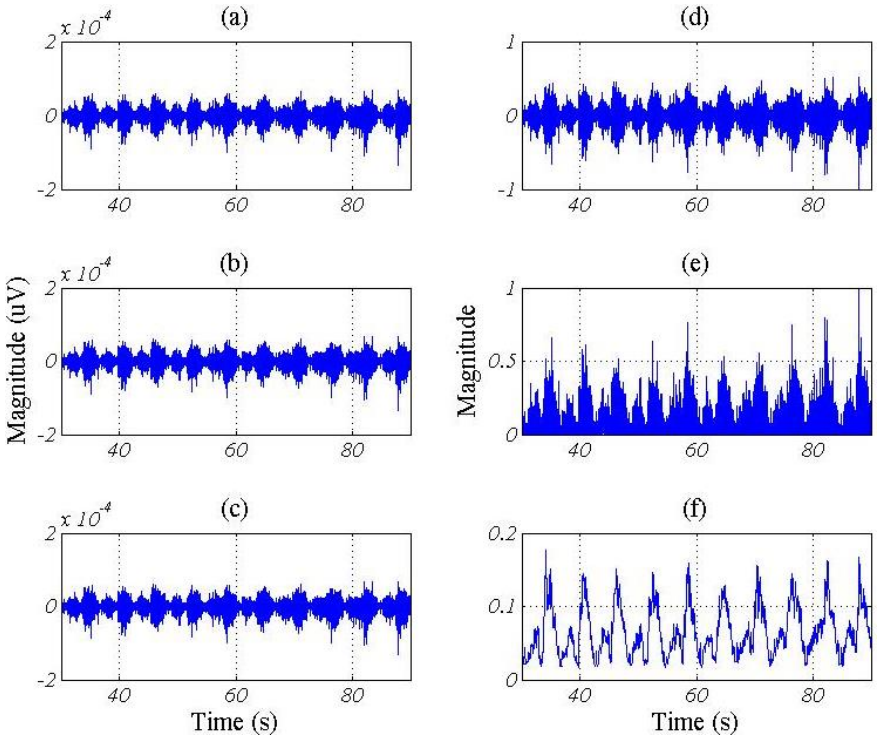

Figure 0.4: sEMG signal processing. (a) Detrended; (b) high pass filtered at 2 Hz; (c) low pass filtered at 450 Hz; (d) normalized; (e) rectified; and (f) low pass filtered at 3 Hz to find envelope.

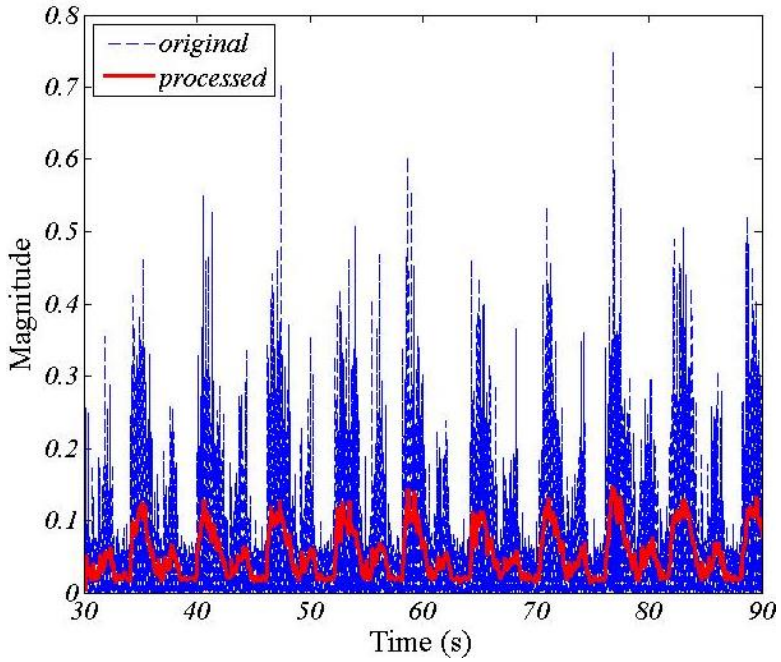

Figure 0.5: Low-pass filtered sEMG comparing with no low-pass filtered signal

The time length of the test was 120 seconds long for each. To eliminate the starting differences and final stage fatigue effects, only the data between 30-90 seconds is shown and used for the comparison. Thus 10 trials data were presented in total. **Figure** 7.6 illustrates the inertial data from the sensors at T_{11} level in both with/without exoskeleton tests from Subject No.1. It needs to be pointed out that when the x axis of the sensor was vertical to the ground, the angle was 90 degrees. Therefore, the two peaks in each trial of the angle shown in the **Figure** 7.6 (a) represented the process of the subject finishing the last trial, passing the neutral position, overshooting backward a little and restarting flexion for another trial. It was also confirmed through the zero cross of the linear acceleration along with the *z* axis in the **Figure** 7.6 (b).

Figure 7.7 illustrates the linear accelerations, $\boldsymbol{a_x}$ and $\boldsymbol{a_z}$, at T_{11} level of Subject No. 1. It shows that the magnitude difference of $\boldsymbol{a_x}$ at full range flexion position was proportional to the difference of flexion angle, indicated from **Figure** 7.6 (a) and 7.7 (a). Plus, the $\boldsymbol{a_x}$ vibrated more when the subject went back to the neutral position because of the spring effects. On the other hand, the $\boldsymbol{a_z}$ with the exoskeleton was markedly larger than the natural body test when the subject flexing. It was because of the pushing forces from the cams on the both sides, and can be quantitatively calculated by the dynamic equation (7-3). The inertial data collected from other subjects were similar with the ones shown in **Figure** 7.6 and 7.7, and they are illustrated in the **Appendix**. These accelerations indicate the reaction forces at the intervertebral joints. Comparing with simulation, the results show that the reaction forces double with optimal spring forces. However, in reality the accelerations shown are much closer wearing with/without exoskeleton. This means that the intervertebral reaction forces are much smaller than in the simulations. This is because of the more complex structures in the human body protect the discs from excessive reaction forces.

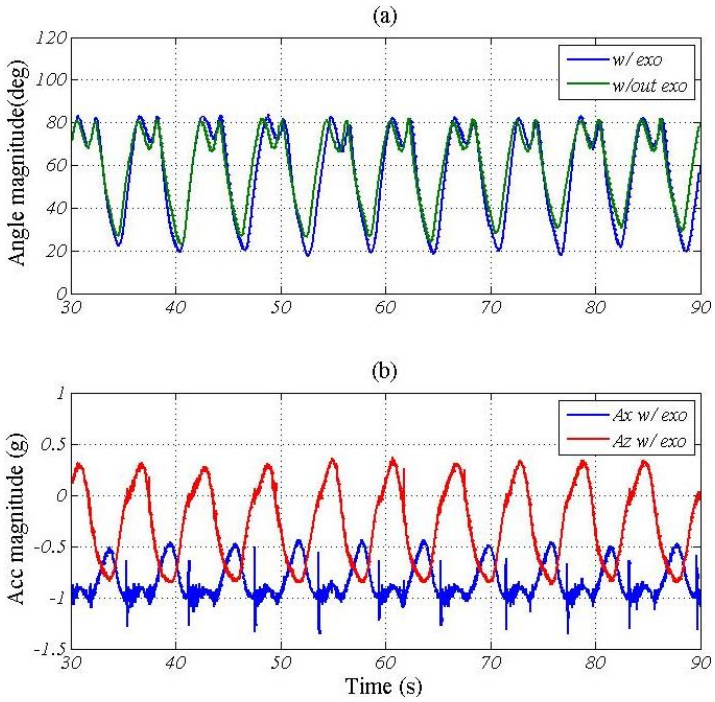

Figure 0.6: (a) Angle comparison from sensor 8 at T_{11} level in both with/without exoskeleton; and (b) linear accelerations on x and z direction with exoskeleton from sensor 7 at T_{11} level

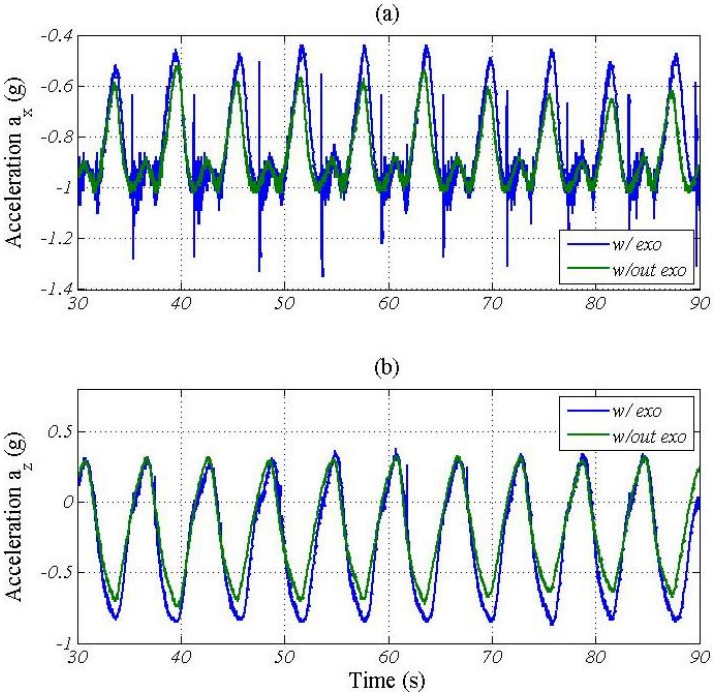

Figure 0.7: The linear accelerations on x and z directions from channel 7 at T_{11} level with/without exoskeleton

The continuous sEMG collected from channel 1, 2, 7 and 8 of Subject No. 1 (continuous sEMG data of Subject No.2 and 3 are shown in the **Appendix**) in the dynamic tests with and without the exoskeleton is shown in **Figure** 7.8. In addition, the trial averages are compared and are shown in **Figure** 7.9 for all three subjects. It shows that the exoskeleton modified the muscle excitation patterns for all subjects. The sEMG magnitudes of thorax muscles were noticeably reduced while sEMG magnitudes of lumbar muscles were slightly less for Subject No. 1 and 3, who have a similar height and weight.

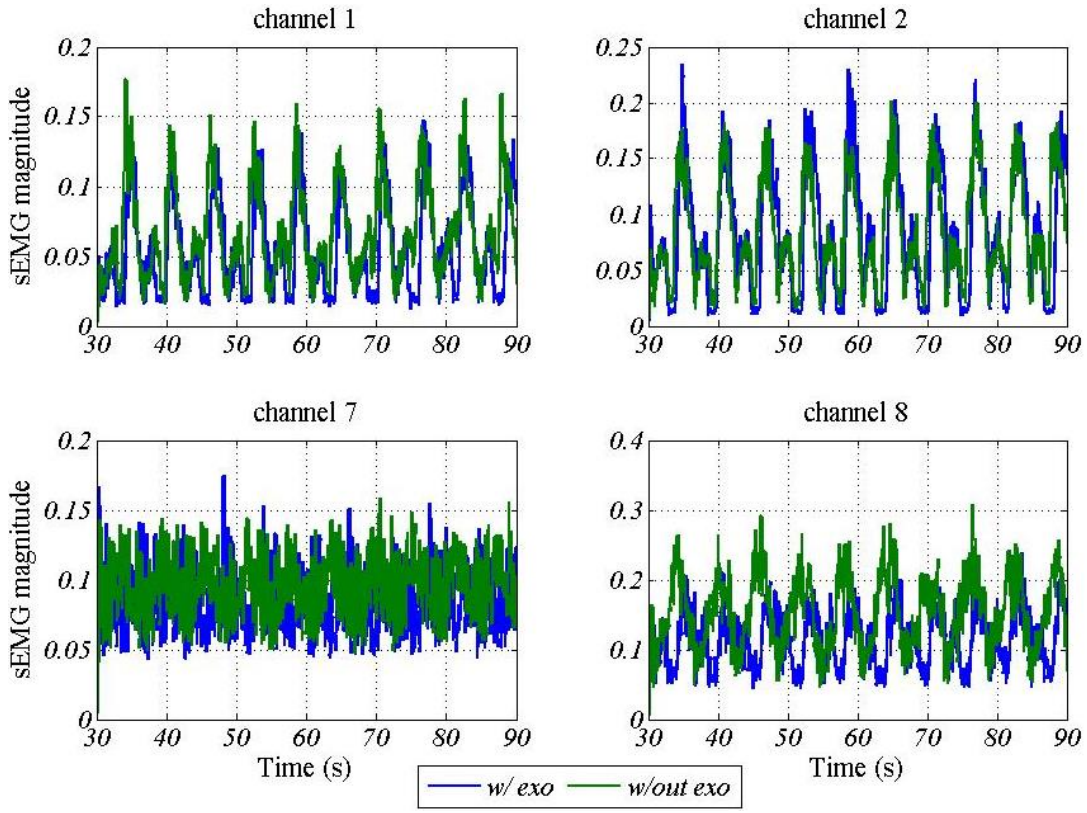

Figure 0.8: sEMG comparison of Subject No. 1 in the dynamic tests with/without exoskeleton – 60-second long continuous sEMG comparison.

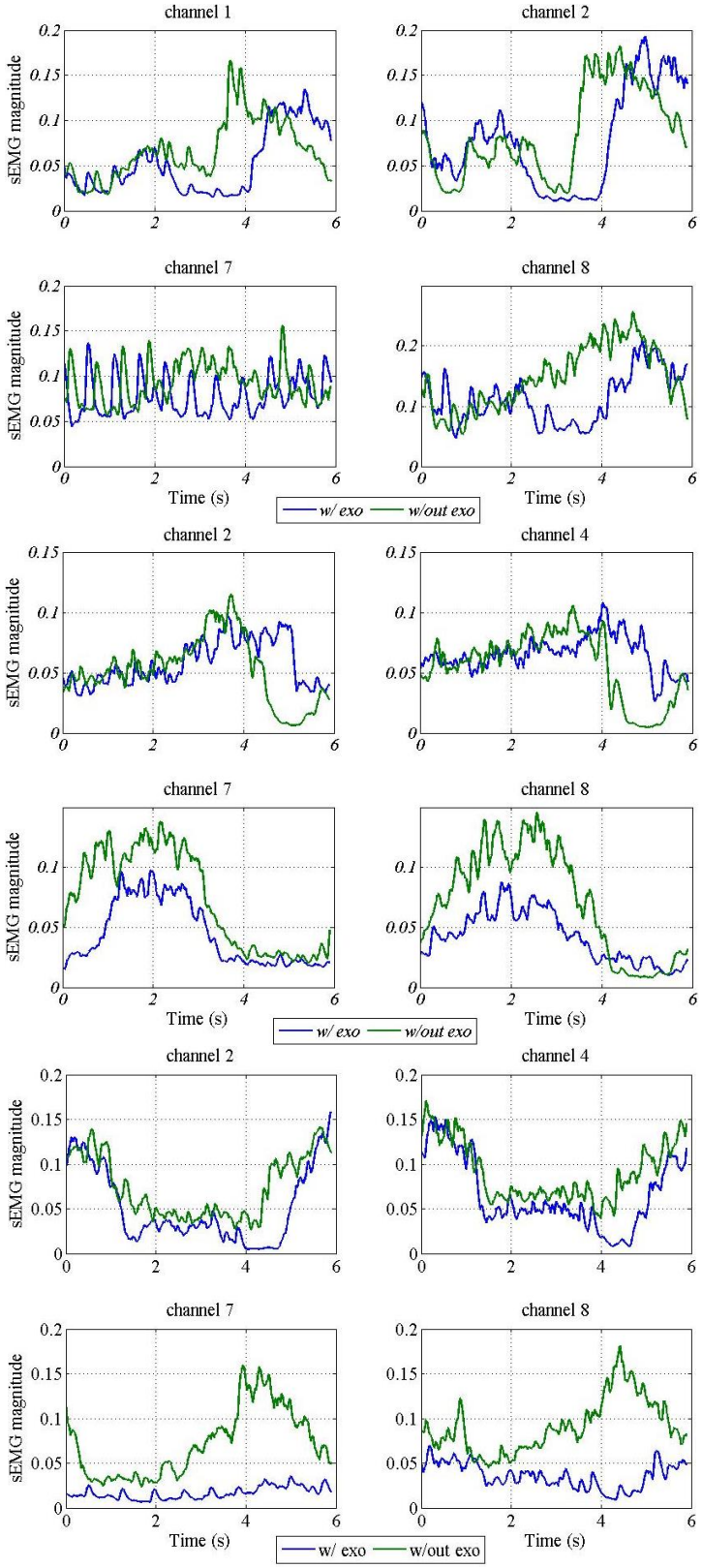

Figure 0.9: sEMG comparison of Subjects in the dynamic tests with/without exoskeleton: (a) Subject No. 1; (b) Subject No. 2; (c) Subject No. 3.

7.4 Results Comparison for Static Tests

Similarly, the results from the static tests were also compared. In each trial of the static tests, the subjects were asked to start from the neutral position and flex over gradually to a certain angle, illustrated in **Figure** 7.2 and **Table** 7.2. This flexion process was accomplished within the first 10 seconds. In addition, each subject extended back slowly to the neutral position in each trial in the last 10 seconds. **Figure** 7.10 showed the comparison of the angle data collected at the T_{11} level in each trial with/without exoskeleton. The steady position in the same static task of the two tests (with and without exoskeleton) were nearly identical. In addition, **Figure** 7.11 illustrated the comparison of the acceleration data collected at the T_{11} level from channel 7, where the $\boldsymbol{a_x}$ were similar while the $\boldsymbol{a_z}$ wearing the exoskeleton were larger than the case without the exoskeleton, which was due to the pressure from the cams during the tests. Furthermore, the sEMG reduction in the static test were compared, shown in **Figure** 7.12 – 7.14 for the data collected in torso Positions 1 to 3 (torso angle reading from **Figure** 7.10 and listed in **Table** 7.4). In the sEMG signals presented in **Figure** 7.12 – 7.14, flexion-relaxation can be observed. According to [27], the sEMG increases with increasing flexion angle and this until reaching about 45 degrees. After that the sEMG magnitude decreases even as flexion angle keeps increasing. This is because with a larger flexion angle, the back muscles stretch and the passive tissues start contracting and providing additional force [1], [27], [32]. Therefore, the sEMG can be an indicator of how much active force is provided by the muscles. The average sEMG reduction of each trial for each subject are listed in **Table** 7.5. The average reduction for all subjects approached 9% at the lumbar level and 40% at the thorax level in test Position 2 (torso angle range 40 – 60 degrees). This means the exoskeleton prototype reduced the muscle activation at the position where the torso requires the

most active muscle support. Further, it indicates that the reductions at the thorax level are generally higher than at the lumbar level for the three subjects.

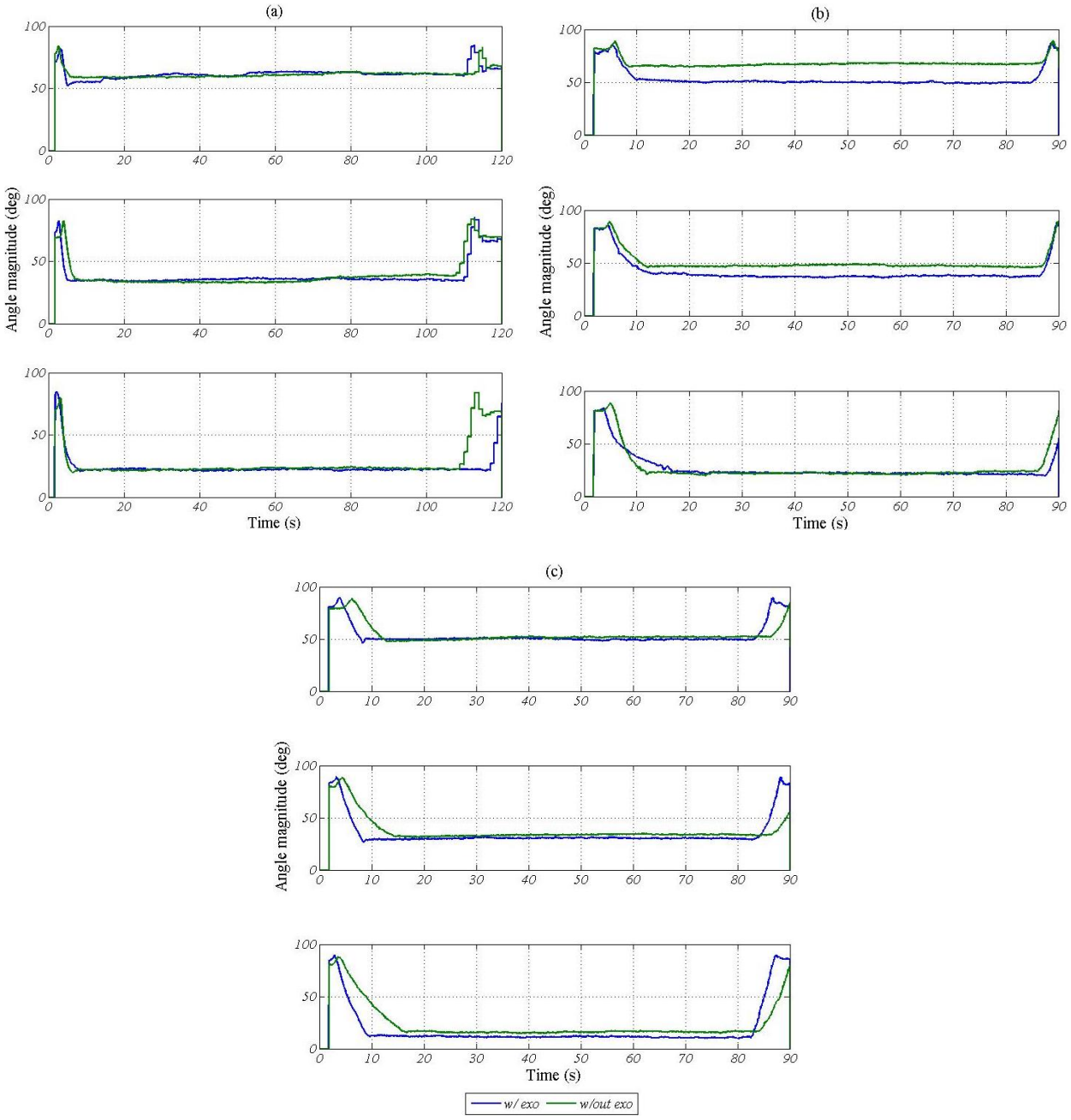

Figure 0.10: Comparison of angle in different static test trials from channel 7: (a) Subject No. 1; (b) Subject No. 2; (c) Subject No. 3.

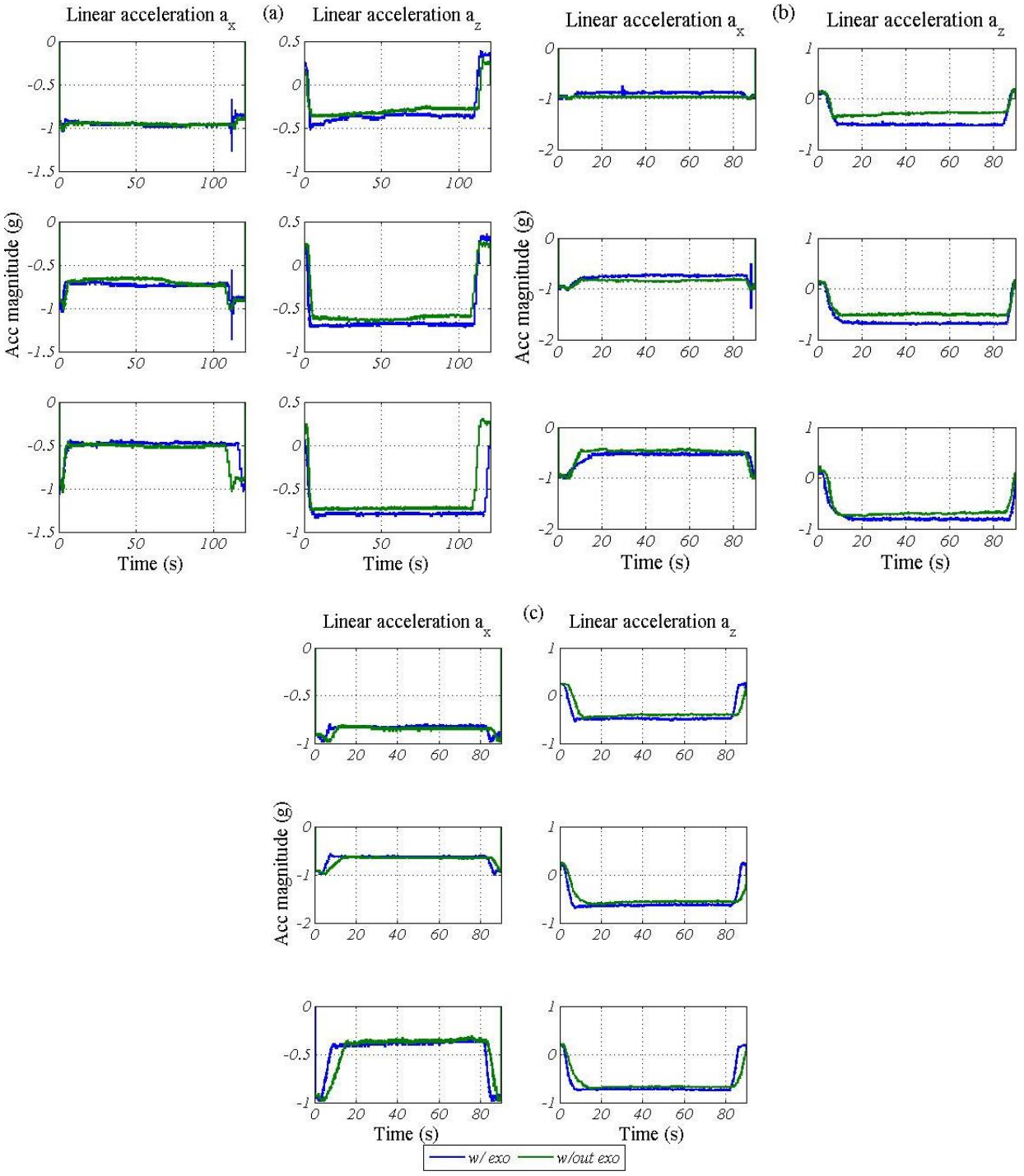

Figure 0.11: Comparison of linear accelerations in different static test trials from channel 7: (a) Subject No. 1; (b) Subject No. 2; (c) Subject No. 3.

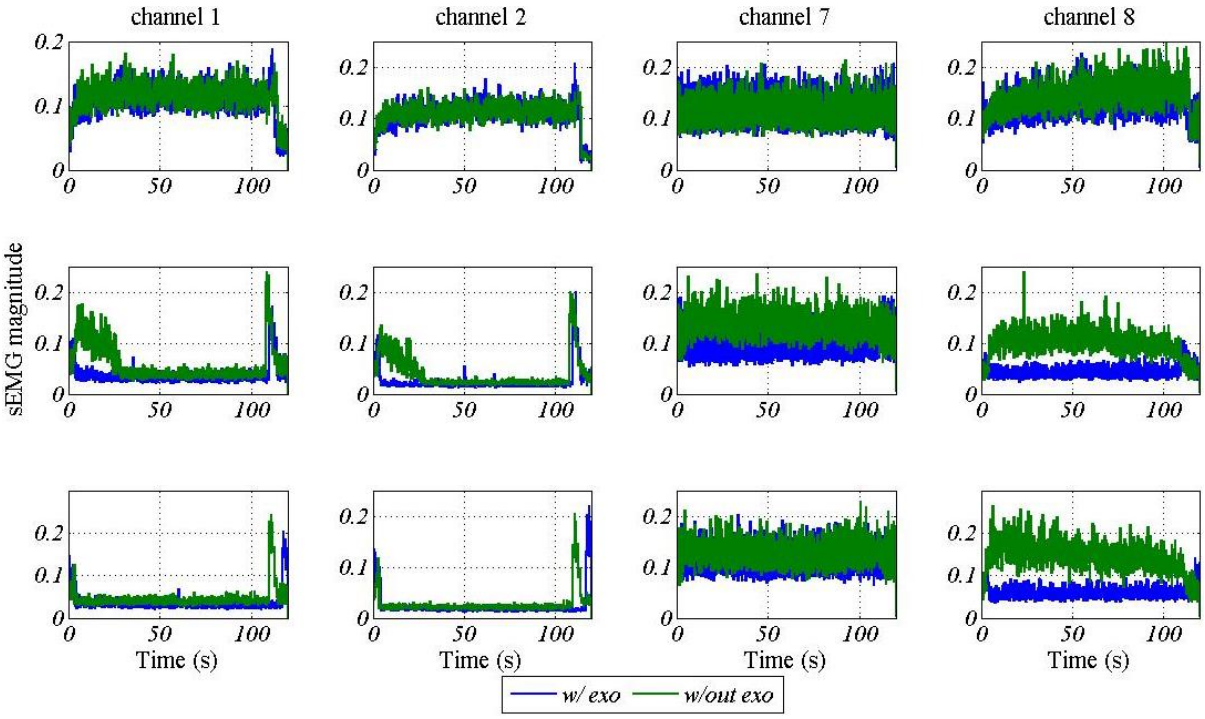

Figure 0.12: Comparison of sEMG in different static test trials of Subject No. 1

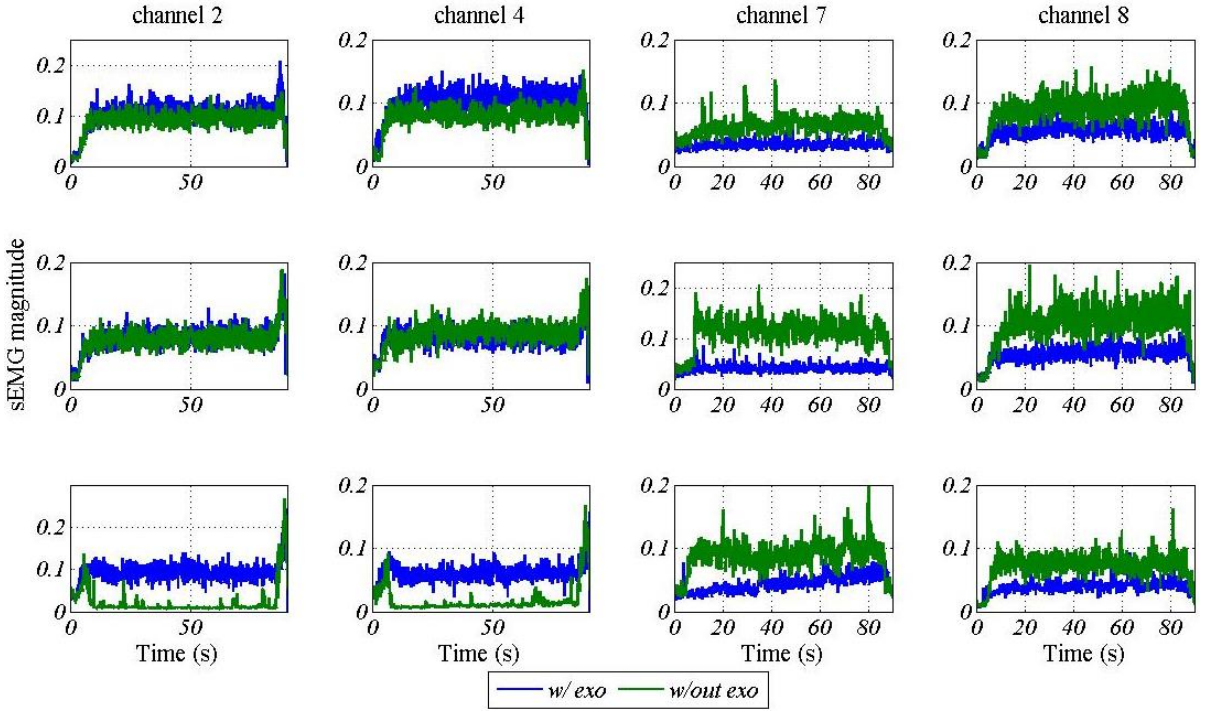

Figure 0.13: Comparison of sEMG in different static test trials of Subject No. 2

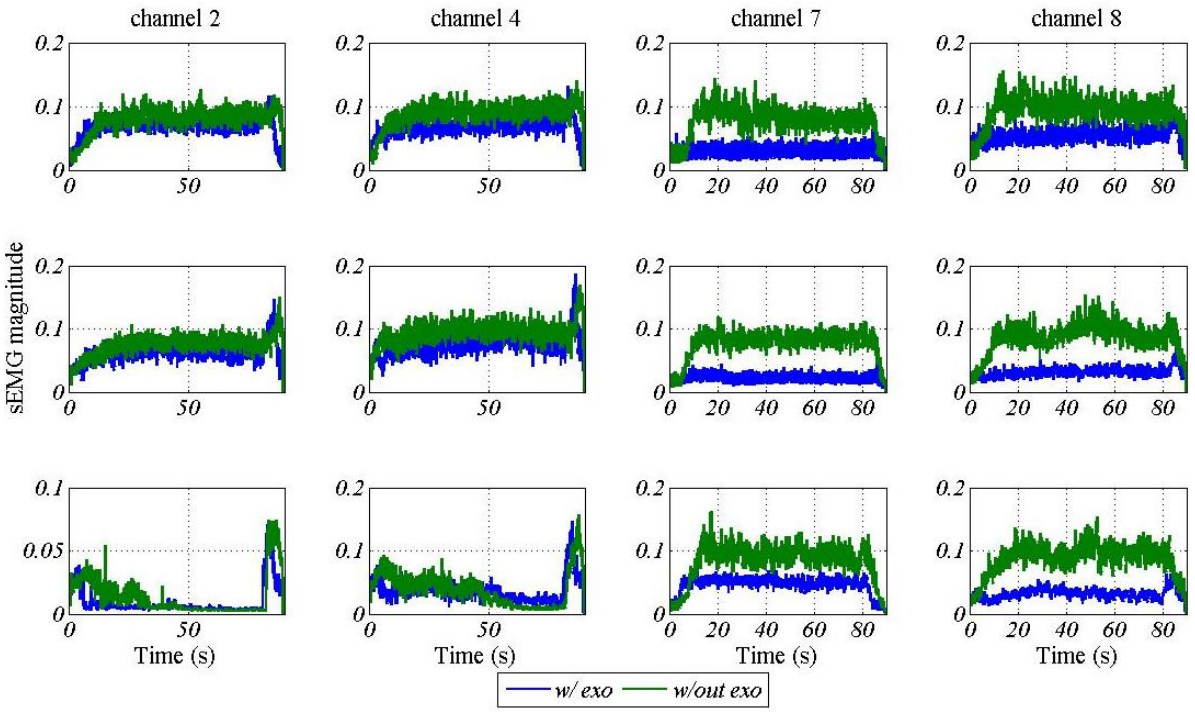

Figure 0.14: Comparison of sEMG in different static test trials of Subject No. 3

Table 0.4: Stable torso bending angle $\boldsymbol{\theta}$ at different positions for each subject (Units: degree). The reference height in **Figure** 7.2 for each subject in different trials are listed in **Table** 7.2.

		Subject No. 1	Subject No. 2	Subject No. 3
Torso Angle @ Position 1	w/out exo	30	23	39
	w/ exo	29	38	40
Torso Angle @ Position 2	w/out exo	55	43	57
	w/ exo	55	53	60
Torso Angle @ Position 3	w/out exo	67	68	74
	w/ exo	68	68	79

Table 0.5: Average percentage of sEMG reduction of each channel for each subject. The largest reductions among all three subjects at lumbar and thorax level muscles are marked bold.

		Position 1	Position 2	Position 3
Subject No. 1	Channel 1 (Right L_3)	0.1%	**17.2%**	**24.3%**
	Channel 2 (Left L_3)	-3.9%	16.7%	17.6%
	Channel 7 (Right T_{11})	-0.3%	26.9%	7.7%
	Channel 8 (Left T_{11})	8.2%	46.0%	**50.0%**
Subject No. 2	Channel 2 (Left L_3)	-16.3%	-0.9%	-39.7%
	Channel 4 (Left L_1)	-17.8%	3.8%	-34.7%
	Channel 7 (Right T_{11})	29.0%	37.2%	21.4%
	Channel 8 (Left T_{11})	22.9%	33.4%	30.9%
Subject No. 3	Channel 2 (Left L_3)	7.1%	8.0%	3.2%
	Channel 4 (Left L_1)	**18.6%**	11.1%	-0.8%
	Channel 7 (Right T_{11})	**42.2%**	**54.1%**	34.6%
	Channel 8 (Left T_{11})	27.1%	44.9%	48.5%
Subject Average	Lumbar Level (L_1&L_3)	-2.0%	9.3%	-5.0%
	Thorax Level (T_{10}&T_{11})	21.5%	40.4%	32.1%

The spring forces were checked in the static tests. **Table** 7.6 – 7.8 list the specific spring forces measured for each spring in each trial for each subject. The spring forces can be calculated in each static position then according to the list of spring constant for each spring. Through the dynamics Equations 7-1 to 7-3, the muscle force reduction and intervertebral reaction torque reduction can be estimated for each subject, which are listed in **Table** 7.9, where the reductions increase with the spring force as well as the increasing flexion angle. In addition, the average reduction in back muscle force and intervertebral reaction torque was measured at 371 N and 29 Nm at Position 3 (torso angle range 65 – 80 degrees), respectively.

In the simulation results from **Chapter** 5 the optimal peak reduction observed with exoskeleton for muscle force and intervertebral reaction torque were 65 N and 37 Nm, respectively. The experimental muscle reduction force is much larger than the one from the simulation. The reason for this is can be attributed to the model using simplified muscle profiles that do not fully capture the complexity of the system. Nevertheless, it should be pointed out that these muscle force reduction from the dynamic analysis might be overestimated and the intervertebral reaction torque

reduction might be underestimated since the estimate neglects the inertial effects of the exoskeleton and underrated the pushing forces by assuming it was parallel to the *z* axis of the sensor. Nevertheless, the design objectives – Back Muscle Effort and Intervertebral Reaction Torque paid by the subjects were both visibly reduced. The results from the Subject No. 3 were similar with the results from the Subject No. 1 who are in almost the same size, while the results from the Subject No. 2 who is much taller indicated several differences. It can be believed that the prototype can provide more assistance for Subject No. 2 since it was designed to their specifications with spring sets and proper prototype dimensions.

Table 0.6: Spring length measurements during the static test of Subject No. 1 (Units: m)

Subject No. 1	Rest length	Neutral Pose	Pose 1	Pose 2	Pose 3	Full flex
Pulling spring 1	0.100	0.100	0.121	0.133	0.139	0.149
Pulling spring 2	0.100	0.100	0.121	0.131	0.135	0.146
Pushing spring 1	0.050	0.050	0.084	0.086	0.106	0.113
Pushing spring 2	0.050	0.050	0.086	0.090	0.102	0.109

Table 0.7: Spring length measurements during the static test of Subject No. 2 (Units: m)

	Neutral Pose	Pose 1	Pose 2	Pose 3
Pulling spring 1	0.100	0.109	0.114	0.123
Pulling spring 2	0.100	0.106	0.112	0.121
Pushing spring 1	0.050	0.069	0.078	0.084
Pushing spring 2	0.050	0.071	0.078	0.084

Table 0.8: Spring length measurements during the static test of Subject No. 3 (Units: m)

	Neutral Pose	Pose 1	Pose 2	Pose 3
Pulling spring 1	0.100	0.113	0.125	0.133
Pulling spring 2	0.100	0.109	0.120	0.131
Pushing spring 1	0.050	0.072	0.087	0.097
Pushing spring 2	0.050	0.079	0.089	0.096

Table 0.9: Result estimation for each subject

		Muscle Force Reduction (N)		Intervertebral Reaction Torque Reduction (Nm)	
Position 1	Subject #1	256	Avg. (143)	12	Avg. (8)
	Subject #2	44		4	
	Subject #3	128		7	
Position 2	Subject #1	397	Avg. (251)	20	Avg. (17)
	Subject #2	104		10	
	Subject #3	252		22	
Position 3	Subject #1	479	Avg. (371)	24	Avg. (29)
	Subject #2	271		27	
	Subject #3	363		36	

CHAPTER 8

CONCLUSION

This thesis proposes a design development process for a passive exoskeleton spine which aimed to reduce both muscular effort and intervertebral reaction torques of the operator. Throughout the research, different models and modeling approaches were applied in the different design phases. The detailed biomechanics computational model was applied in OpenSim to provide accurate design guidance. Then the mathematical spine model was developed from the musculoskeletal model and the "push-pull" assistive strategy was proposed. In addition, to evaluate the "push-pull", a biomechanics model associating several simple geometry was built up back in OpenSim and evaluated via the simulation process. A 3-D model was designed to implement the "push-pull" obtained from the simulations. The final prototype was tested with human subjects.

The major contributions of this thesis include: (1) proposed a method for design human-machine interaction leading by biomechanics simulations, (2) a "push-pull" strategy for assisting human being sagittal plane spine flexion/extension, and (3) a passive exoskeleton spine test platform.

The design method was developed based on biomechanics simulation platform –OpenSim. It provides accurate and visible details biomechanics process of the muscular skeleton during the specific movement. It only needs kinematics data collected from healthy subject and does not need human subject to be involved during the prototype design period, which ensures the design process much more secure and remarkably curtails the design period. The spring constant optimization process introduced in this thesis is based on non-preference. This allows the reduction of muscle forces and intervertebral torques to be balanced by changing the weights of the design objectives.

The "push-pull" strategy was evaluated through simulation model, which provided an instruction of how to effectively apply external loading on the human torso. The optimal design in the simulations indicated a 16% (65 N) peak reduction and a 31% mean reduction with respect to the Back Muscle Effort, while a 71% (37 Nm) peak reduction and 78% mean reduction with respect to the Intervertebral Reaction Torque. In simulation, a side effect of the "push-pull" external assistive strategy was an increase in the intervertebral reaction forces.

The prototype was tested on three human subjects, which offered the first implementation of the "push-pull" strategy. The prototype evaluations indicated the positive effect of the "push-pull" by sEMG reductions and estimated reductions of Back Muscle Effort and Intervertebral Reaction Torque. It turned out that the sEMG reductions can reach 54% peak (average 40%) and 17% peak (average 9%) at thorax and lumbar level muscles at torso angle around 45 degrees, where the flexion-relaxation phenomenon is about to happen. In addition, the Back Muscle Effort and Intervertebral Reaction Torque reduced 479 N peak (average 371 N) and 36 N peak (average 29 N) at a torso angle of 65 degrees. In terms of the Intervertebral Reaction Torque, the estimation results matched well with the results from the simulations. The estimated reductions for muscle forces did not align as well due to the complexity of the muscles not captured in the simplified muscle groups used in simulation.

This thesis presented a design of a passive exoskeleton spine. The mechanism along with the "push-pull" external assist strategy has been successfully tested in simulations and prototype. The exoskeleton is potentially activated by external actuators to realize fully external assists. In addition, once the active exoskeleton platform is constructed, adaptive control schemes can be applied to control the exoskeleton according to the user intent and smoothen the movements. What

is more, this upper body exoskeleton can be used to combine the works on the lower limb exoskeletons to realize full body external assists in the future.

APPENDIX

FULL DYNAMIC TESTING RESULTS FOR SUBJECTS NO. 2 AND 3

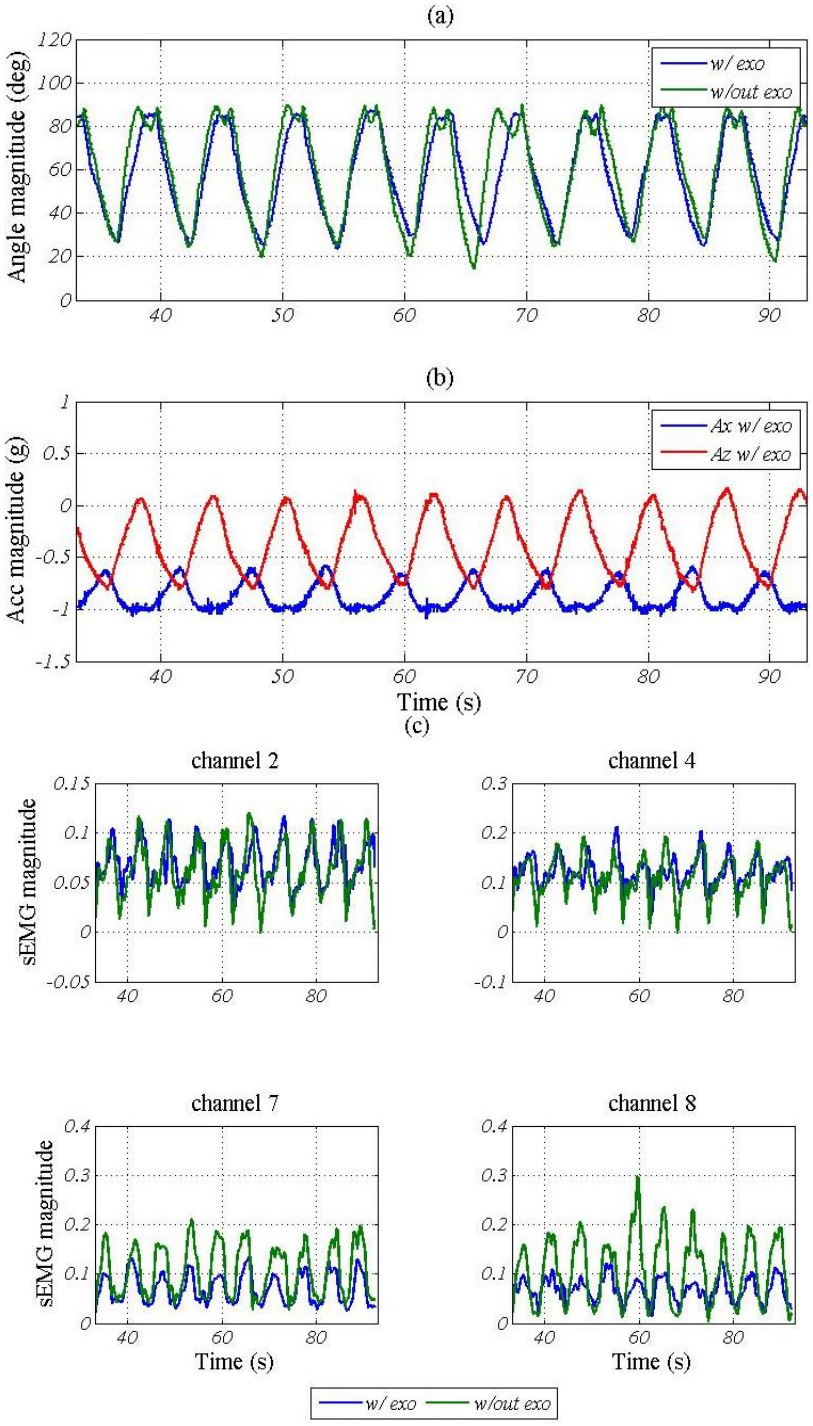

Figure A.1: Results comparisons of dynamic tests for Subject No.2: (a) angle comparison at T_{11} level; (b) linear accelerations at T_{11} level wearing exoskeleton; (c) sEMG comparison at channel 2, 4, 7 and 8.

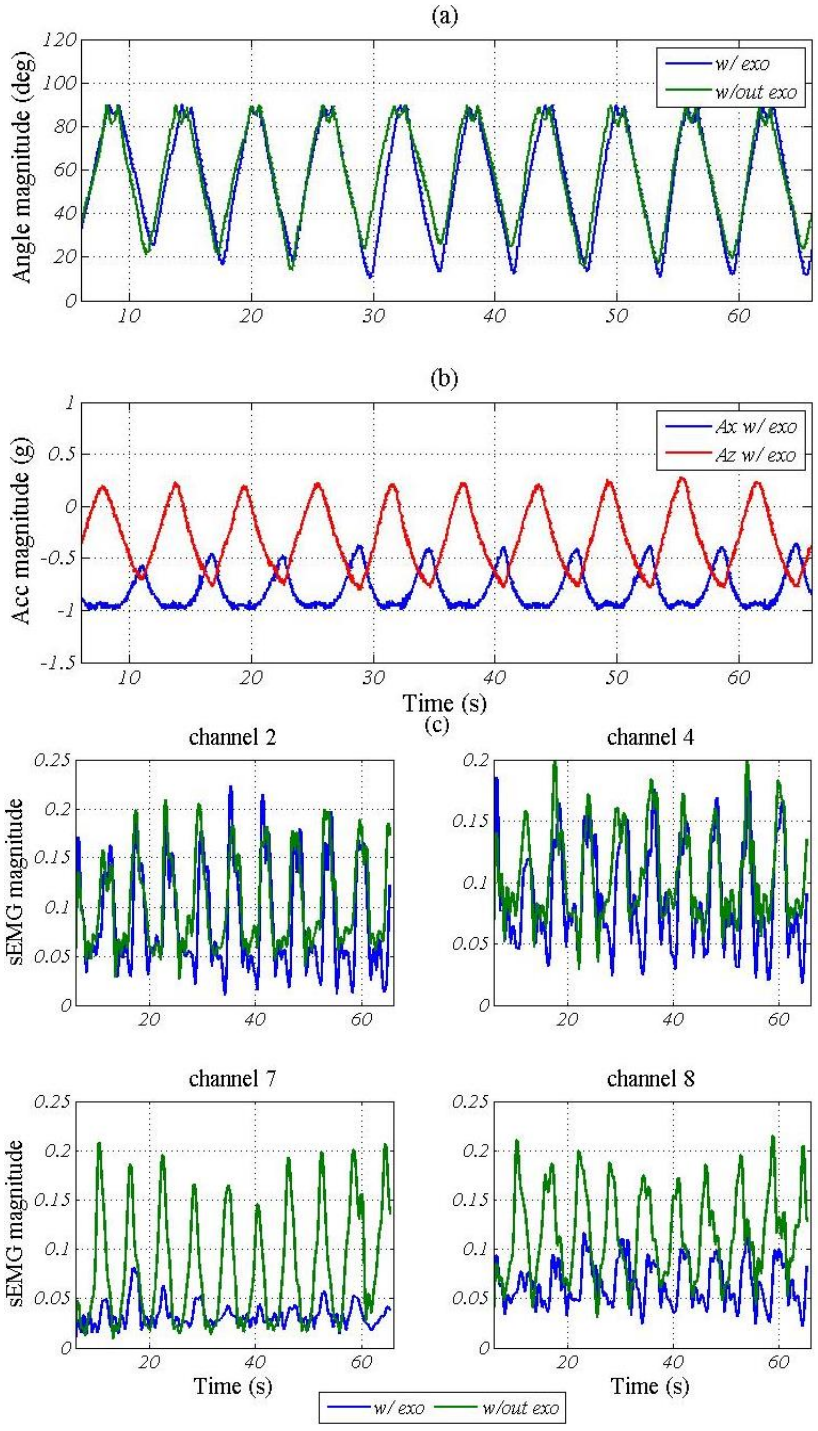

Figure A.2: Results comparisons of dynamic tests for Subject No.3: (a) angle comparison at T_{11} level; (b) linear accelerations at T_{11} level wearing exoskeleton; (c) sEMG comparison at channel 2, 4, 7 and 8.

BIBLIOGRAPHY

[1] M. a Adams, N. Bogduk, B. Kim, P. Dolan, and B. j c Freeman, *The Biomechanics of Back Pain*, 3rd ed., vol. 22, no. 4. Elsevier, 2013.

[2] C.-K. Cheng, H.-H. Chen, H.-H. Kuo, C.-L. Lee, W.-J. Chen, and C.-L. Liu, "A three-dimensional mathematical model for predicting spinal joint force distribution during manual liftings.," *Clin. Biomech. (Bristol, Avon)*, vol. 13, no. 1 Suppl 1, pp. S59–S64, Jan. 1998.

[3] M. a Adams and P. Dolan, "A technique for quantifying the bending moment acting on the lumbar spine in vivo.," *Journal of biomechanics*, vol. 24, no. 2. pp. 117–26, Jan-1991.

[4] a Shirazi-Adl and M. Parnianpour, "Load-bearing and stress analysis of the human spine under a novel wrapping compression loading.," *Clin. Biomech. (Bristol, Avon)*, vol. 15, no. 10, pp. 718–25, Dec. 2000.

[5] N. Arjmand, D. Gagnon, a Plamondon, a Shirazi-Adl, and C. Larivière, "Comparison of trunk muscle forces and spinal loads estimated by two biomechanical models.," *Clin. Biomech. (Bristol, Avon)*, vol. 24, no. 7, pp. 533–41, Aug. 2009.

[6] M. Christophy, "A Detailed Open-Source Musculoskeletal Model of the Human Lumbar Spine by," 2010.

[7] M. Christophy, N. A. Faruk Senan, J. C. Lotz, and O. M. O'Reilly, "A musculoskeletal model for the lumbar spine.," *Biomech. Model. Mechanobiol.*, vol. 11, no. 1–2, pp. 19–34, Jan. 2012.

[8] H. Hara and Y. Sankai, "HAL equipped with passive mechanism," *2012 IEEE/SICE Int. Symp. Syst. Integr.*, pp. 1–6, Dec. 2012.

[9] A. L. Rosatelli, K. Ravichandiran, and A. M. Agur, "Three-dimensional study of the musculotendinous architecture of lumbar multifidus and its functional implications.," *Clin. Anat.*, vol. 21, no. 6, pp. 539–46, Sep. 2008.

[10] M. M. Panjabi, "The stabilizing system of the spine. Part I. Function, dysfunction, adaptation, and enhancement.," *Journal of spinal disorders*, vol. 5, no. 4. pp. 383–9; discussion 397, Dec-1992.

[11] K. W. N. Wong, K. D. K. Luk, J. C. Y. Leong, S. F. Wong, and K. K. Y. Wong, "Continuous dynamic spinal motion analysis.," *Spine*, vol. 31, no. 4. pp. 414–9, 15-Mar-2006.

[12] D. Gagnon, C. Larivière, and P. Loisel, "Comparative ability of EMG, optimization, and hybrid modelling approaches to predict trunk muscle forces and lumbar spine loading

during dynamic sagittal plane lifting.," *Clin. Biomech. (Bristol, Avon)*, vol. 16, no. 5, pp. 359–72, Jun. 2001.

[13] A. Seth, M. Sherman, J. a. Reinbolt, and S. L. Delp, "OpenSim: a musculoskeletal modeling and simulation framework for in silico investigations and exchange," *Procedia IUTAM*, vol. 2, pp. 212–232, Jan. 2011.

[14] S. L. Delp, F. C. Anderson, A. S. Arnold, P. Loan, A. Habib, C. T. John, E. Guendelman, and D. G. Thelen, "OpenSim: open-source software to create and analyze dynamic simulations of movement.," *IEEE Trans. Biomed. Eng.*, vol. 54, no. 11, pp. 1940–50, Nov. 2007.

[15] H. Kazerooni, J. Racine, L. Huang, and R. Steger, "On the Control of the Berkeley Lower Extremity Exoskeleton (BLEEX)," no. April, pp. 4353–4360, 2005.

[16] E. E. Bleex, A. B. Zoss, H. Kazerooni, and A. Chu, "Biomechanical Design of the Berkeley Lower," vol. 11, no. 2, pp. 128–138, 2006.

[17] S. Lee and Y. Sankai, "The natural frequency-based power assist control for lower body with HAL-3," *SMC'03 Conf. Proceedings. 2003 IEEE Int. Conf. Syst. Man Cybern. Conf. Theme - Syst. Secur. Assur. (Cat. No.03CH37483)*, vol. 2, pp. 1642–1647.

[18] T. Hayashi, H. Kawamoto, and Y. Sankai, "Control method of robot suit HAL working as operator's muscle using biological and dynamical information," *2005 IEEE/RSJ Int. Conf. Intell. Robot. Syst.*, vol. 2, no. 1, pp. 3063–3068, 2005.

[19] S. R. Taal and Y. Sankai, "Exoskeletal Spine and Shoulders for Full Body Exoskeletons in Health Care," vol. 2, no. 6, pp. 270–286, 2011.

[20] Y. Sankai, "Leading Edge of Cybernics: Robot Suit HAL," *2006 SICE-ICASE Int. Jt. Conf.*, vol. 10, p. P–1–P–2, 2006.

[21] "Second Spine." [Online]. Available: http://carnot.mech.columbia.edu/~rrl/projects/secondSpine/.

[22] T. Kozuki, H. Mizoguchi, Y. Asano, M. Osada, T. Shirai, U. Junichi, Y. Nakanishi, K. Okada, and M. Inaba, "Design Methodology for the Thorax and Shoulder of Human Mimetic Musculoskeletal Humanoid Kenshiro -A Thorax structure with Rib like Surface -," pp. 3687–3692, 2012.

[23] Y. Asano, H. Mizoguchi, T. Kozuki, Y. Motegi, M. Osada, J. Urata, Y. Nakanishi, K. Okada, and M. Inaba, "Lower thigh design of detailed musculoskeletal humanoid 'Kenshiro,'" *2012 IEEE/RSJ Int. Conf. Intell. Robot. Syst.*, pp. 4367–4372, Oct. 2012.

[24] Y. N. S. Ohta, “Design Approach of Biologically-Inspired Musculoskeletal Humanoids.” [Online]. Available: http://cdn.intechopen.com/pdfs/44420/InTech-Design_approach_of_biologically_inspired_musculoskeletal_humanoids.pdf.

[25] A. Ananthanarayanan, M. Azadi, and S. Kim, “Towards a bio-inspired leg design for high-speed running.,” *Bioinspiration & biomimetics*, vol. 7, no. 4. p. 046005, Dec-2012.

[26] G. a. Folkertsma, S. Kim, and S. Stramigioli, “Parallel stiffness in a bounding quadruped with flexible spine,” *2012 IEEE/RSJ Int. Conf. Intell. Robot. Syst.*, pp. 2210–2215, Oct. 2012.

[27] a B. Schultz, K. Haderspeck-Grib, G. Sinkora, and D. N. Warwick, “Quantitative studies of the flexion-relaxation phenomenon in the back muscles.,” *Journal of orthopaedic research : official publication of the Orthopaedic Research Society*, vol. 3, no. 2. pp. 189–97, Jan-1985.

[28] J. H. Skotte, “Estimation of low back loading on nurses during patient handling tasks: the importance of bedside reaction force measurement.,” *J. Biomech.*, vol. 34, no. 2, pp. 273–6, Feb. 2001.

[29] K. P. Granata, P. E. Lee, and T. C. Franklin, “Co-contraction recruitment and spinal load during isometric trunk flexion and extension.,” *Clin. Biomech. (Bristol, Avon)*, vol. 20, no. 10, pp. 1029–37, Dec. 2005.

[30] B. Y. R. V. A. N. Ham, T. G. Sugar, B. Vanderborght, K. W. Hollander, and D. Lefeber, “Review of Actuators with Passive Adjustable Compliance/Controllable Stiffness for Robotic Applications,” no. September, pp. 81–94, 2009.

[31] D. W. Robinson, “Design and Analysis of Series Elasticity in Closed-loop Actuator Force Control by,” 2000.

[32] C. J. Colloca and R. N. Hinrichs, “The biomechanical and clinical significance of the lumbar erector spinae flexion-relaxation phenomenon: a review of literature.,” *J. Manipulative Physiol. Ther.*, vol. 28, no. 8, pp. 623–31, Oct. 2005.